Tensor Networks for Solving Realistic Time-independent Boltzmann Neutron Transport Equation

Duc P. Truong^a, Mario I. Ortega^b, Ismael Boureima^a, Gianmarco Manzini^a, Kim Ø. Rasmussen^a, and Boian S. Alexandrov^a

^a Theoretical Division, Los Alamos National Laboratory, Los Alamos, New Mexico
^b Computer, Computational, and Statistical Sciences Division, Los Alamos National Laboratory, Los Alamos, New Mexico

Abstract

Tensor network techniques, known for their low-rank approximation ability that breaks the curse of dimensionality, are emerging as a foundation of new mathematical methods for ultra-fast numerical solutions of high-dimensional Partial Differential Equations (PDEs). Here, we present a mixed Tensor Train (TT)/Quantized Tensor Train (QTT) approach for the numerical solution of time-independent Boltzmann Neutron Transport equations (BNTEs) in Cartesian geometry. Discretizing a realistic three-dimensional (3D) BNTE by (i) diamond differencing, (ii) multigroup-in-energy, and (iii) discrete ordinate collocation leads to huge generalized eigenvalue problems that generally require a matrix-free approach and large computer clusters. Starting from this discretization, we construct a TT representation of the PDE fields and discrete operators, followed by a QTT representation of the TT cores and solving the tensorized generalized eigenvalue problem in a fixed-point scheme with tensor network optimization techniques. We validate our approach by applying it to two realistic examples of 3D neutron transport problems, currently solved by the PARallel TIme-dependent SN (PARTISN) solver¹. We demonstrate that our TT/QTT method, executed on a standard desktop computer, leads to a yottabyte compression of the memory storage, and more than 7500 times speedup with a discrepancy of less than 10^{-5} when compared to the PARTISN solution.

Keywords: 2020 Mathematics Subject Classification: Primary: 65M60, 65N30; Secondary: 65M22.

1. Introduction

Realistic simulations in classical and quantum physics and chemistry and complex engineering problems often seek numerical solutions of high-dimensional partial differential equations (PDEs) or integro-differential equations. To numerically solve such equations, discretized versions of the mathematical models are required. The discretization represents the solution, a multivariate function, by its values at a number of grid points and the derivatives of this function through differences in these values.

The number of grid points increases exponentially with the number of dimensions, d, often making numerical solutions infeasible. This phenomenon is called the *curse of dimensionality* [8],

¹The "SN method" (structured Newton method) is an approximation method for solving the radiation transport equation by discretizing both the XYZ-domain and the angular variables that specify the direction of radiation, developed by Subrahmanyan Chandrasekhar.

it causes the poor computational scaling of numerical algorithms, and is the primary challenge for multidimensional numerical computations regardless of the specific problem. Importantly, exascale high-performance computing, which offers strategies for optimization, cannot break the curse of dimensionality.

A very recent and promising approach to mitigate or even remove the curse of dimensionality is based on Tensor Networks (TNs), which represent a non-trivial generalization of tensor factorization. In big data analytics, TNs allow the examination of high-dimensional data by partitioning them into smaller, manageable blocks, i.e., by approximating a high-dimensional array by a network of low-dimensional tensors. In this sense, we can consider classical tensor factorization formats such as Canonical Polyadic Decomposition (CPD) and Tucker decomposition as TNs. Tensor networks (TNs), which are multilinear-algebra data structures [4, 13], have been developed and enjoyed great success in theoretical physics [17, 22, 49], as well as in data science in machine learning [12, 14]. TNs are emerging as a promising novel strategy for breaking the curse of dimensionality [25] in the numerical solution of high-dimensional differential equations and integrals [3, 24, 32]. Several authors have recently used TNs seeking fast and accurate solutions of specific examples of equations, such as the Poisson equation [11], the Schrödinger equation [23], the Poisson-Boltzmann equation [36], the Smoluchowski equation [39, 42], the Maxwell equations [40], the Vlasov-Poisson equations [34], the neutron diffusion equation [35], and others.

Numerical algorithms for solving PDEs are, in general, composed of two main ingredients. The first one is the *grid functions*, which are the value of the functions evaluated at the nodes of a discrete grid. The second ingredient is given by the *discrete operators*, which are the discrete analogs of differential operators (e.g., gradient, curl, divergence), a combination of them (e.g., Laplacian, div-grad, etc), and numerical interpolation and integration operators.

The Boltzmann Neutron Transport Equation (BNTE) [37] is an integro-differential equation for the neutron angular flux describing the location in space, energy, and the direction of neutrons in a physical system of interest, such as a nuclear reactor. The BNTE discretization is driven by the physics of neutron interactions and generates extremely large linear systems of equations that cannot be straightforwardly handled numerically. Here, we introduce a new approach to solving the BNTE, which is based on the Tensor Train (TT) format [46] combined with the Quantized Tensor Train (QTT) format [31], and applied to the finite difference discretization method. This discretization approach leads to ultra-large linear systems of equations and generalized eigenvalue problems. TT solvers exists to solve linear systems in TT format. Examples are the Alternating Linear Scheme (ALS) [28], the Density Matrix Renormalization Group Algorithm (DMRG) [51], the Alternating Minimal Energy (AMEn) methods [19], etc. In contrast, methods for solving eigenvalue problems in TT/QTT format are still an open research topic with a few algorithms being proposed [18, 50]. In this work, we do not utilize a linear solver based on Krylov subspaces but instead, we seek the solution directly in the TT format [47], while we redesign a fixed-point scheme in the QTT format to compute the largest eigenvalue of the BNTE problem. We compare the efficiency, speed, memory requirements, and accuracy, of our method to the traditional matrix-free approach [58] for solving realistic BNTEs for three-dimensional systems [43]. We demonstrate that our TT/QTT method can give us a more than 7500 times speedup. based on yottabyte compression, while preserving an accuracy of 10^{-5} .

The outline of the paper is as follows. In Section 2.1, we review some basic concepts and the matrix formulation of the Boltzmann Neutron Transport Equation that leads to a generalized eigenvalue problem. In Section 2.2, we introduce the tensor notation and the definitions of tensor networks, TT and QTT formats, and their application to PDEs. In Section 3.1, we present our TT/QTT design of the numerical solution of the Boltzmann Neutron Transport Equation and introduce our fixed-point algorithms in tensor train format.

In Section 3.5, we present our numerical results and assess the performance of our method, comparing its efficiency to the efficiency of the PARallel TIme Dependent SN (PARTISN) solver [1] applied to the same problems. In Section 4, we offer our final remarks and discusses possible future work.

For completeness, we report part of the details the BNTE matrix representation in Appendix A and details of the tensorization approach in Appendix B.

2. Methods

2.1. Boltzmann Neutron Transport Equation

In the design of nuclear systems such as nuclear reactors, nuclear engineers are especially interested in determining the criticality conditions. Criticality is the ability of a nuclear system to sustain a nuclear chain reaction (number of neutrons created in fission is equal to the number of neutrons lost in the system) without an external source [7]. To determine the criticality of a system, we consider the time-independent, k-effective eigenvalue problem and the alphaeffective eigenvalue problem for the eigenpairs (k_{eff}, ψ) and (α, ψ) . Both eigenvalue problems provide helpful insight into nuclear systems and are used throughout nuclear reactor design and dynamics, criticality safety, and nuclear non-proliferation applications. In both cases, the eigenfunction ψ is a function of the position vector \mathbf{r} , the direction variable is $\hat{\Omega}$, and the group energy E, i.e., $\psi(\mathbf{r}, \hat{\Omega}, E)$. The position vector \mathbf{r} varies on the space domain

$$\mathcal{D} \equiv \left\{ \mathbf{r} = (x, y, z) \in \mathbb{R}^3 | a_x \le x \le b_x, a_y \le y \le b_y, a_z \le z \le b_z \right\},\,$$

where $[a_x, b_x]$,, $[a_y, b_y]$,, $[a_z, b_z]$ are bounded subintervals of \mathbb{R} ; the direction variable $\hat{\Omega}$ varies on \mathcal{S}^2 , the unit sphere in \mathbb{R}^3 ; the energy group varies, for convenience, between a minimum and maximum values, e.g., $E \in [E_{\min}, E_{\max}]$. For both problems, we assume vacuum Dirichlet boundary conditions:

$$\psi(\mathbf{r}, \hat{\Omega}, E) = 0 \text{ for all } \mathbf{r} \in \partial \mathcal{D} \text{ and } \hat{\Omega} \in \mathcal{S}^2 \text{ with } \mathbf{n}(\mathbf{r}) \cdot \hat{\Omega} < 0,$$
 (2.1)

where $\mathbf{n}(\mathbf{r})$ is the unit normal vector to $\partial \mathcal{D}$, the boundary of the computational domain \mathcal{D} , and pointing out of \mathcal{D}

In both eigenvalue problems, the physics of neutron interactions with matter is captured through neutron cross sections, probabilistic measures of certain nuclear reactions taking place [20] The cross section are denoted as σ , σ_s , σ_f , the total, scattering, and fission cross sections, respectively, and are functions of material, energy, and collision angle. We also use the symbol ν to denote the number of neutrons emitted in fission, while $\chi(E' \to E)$ denotes the probability distribution function expressing the probability that a neutron with energy E' induces fission on fissile nuclei and creates neutrons with energy E.

2.1.1. The k-effective eigenvalue problem

For the eigenpair (k_{eff}, ψ) , we consider the eigenvalue problem

$$\hat{\Omega} \cdot \nabla \psi(\mathbf{r}, \hat{\Omega}, E) + \sigma(\mathbf{r}, E) \psi(\mathbf{r}, \hat{\Omega}, E)
= \int_{\mathcal{S}^2} d\hat{\Omega}' \, \psi(\mathbf{r}, \hat{\Omega}', E) \sigma_s(\mathbf{r}, \hat{\Omega} \cdot \hat{\Omega}', E)
+ \frac{1}{k_{\text{eff}}} \int_0^\infty dE' \int_{\mathcal{S}^2} d\hat{\Omega}' \chi(E' \to E) \nu \sigma_f(\mathbf{r}, E') \psi(\mathbf{r}, \hat{\Omega}', E').$$
(2.2)

In (2.2), the eigenvalue k_{eff} scales the number of neutrons emitted in fission, and its value determines the criticality of the system:

$$k_{\mathrm{eff}} \quad \left\{ egin{array}{ll} > 1, & \mathrm{supercritical}, \\ = 1, & \mathrm{critical}, \\ < 1, & \mathrm{subcritical}. \end{array}
ight.$$

A system with $k_{\text{eff}} = 1$ is considered critical and the number of neutrons is constant in time. The number of neutrons goes to zero or infinity for subcritical or supercritical systems, respectively.

2.1.2. The alpha-effective eigenvalue problem

For the eigenpair (α, ψ) , we consider the eigenvalue problem

$$\frac{\alpha}{v(E)}\psi(\mathbf{r},\hat{\Omega},E) + \hat{\Omega}\cdot\nabla\psi(\mathbf{r},\hat{\Omega},E) + \sigma(\mathbf{r},E)\psi(\mathbf{r},\hat{\Omega},E)
= \int_{\mathcal{S}^2} d\hat{\Omega}'\,\psi(\mathbf{r},\hat{\Omega}',E)\sigma_s(\mathbf{r},\hat{\Omega}\cdot\hat{\Omega}',E)
+ \int_0^\infty dE' \int_{\mathcal{S}^2} d\hat{\Omega}'\chi(E'\to E)\nu\sigma_f(\mathbf{r},E')\psi(\mathbf{r},\hat{\Omega}',E').$$
(2.3)

The alpha-eigenvalue α gives a measure of the asymptotic time behavior of a system and can also be used to determine the criticality of a system:

$$\alpha \begin{cases} > 0, & \text{supercritical,} \\ = 0, & \text{critical,} \\ < 0, & \text{subcritical.} \end{cases}$$

For supercritical systems, the alpha-eigenvalue is the e-folding time for the neutron angular flux in a nuclear system, i.e., the time interval in which ψ grows exponentially by a factor of e.

2.1.3. Discretization of the Three-Dimensional Neutron Transport

The numerical solution of equations (2.2) and (2.3) requires discretization along the spatial, angular, and energy variables. In this section, we describe the major discretization issues and the matrix formulation, which is similar to that of Refs. [9] and [44]. Specifically, we first consider the energy variable; then, the angular variable; and, finally, the space variables.

2.1.4. Discrete formulation of k-effective and alpha-effective eigenvalue problems

The discretized forms of equations (2.2) and (2.3) are (see Appendix A for details):

$$\frac{\mu_{\ell}}{4\Delta x_{i}} \left[\sum_{k'=k-1}^{k} \sum_{j'=j-1}^{j} \psi_{g,\ell,k',j',i} - \psi_{g,\ell,k',j',i-1} \right] + \frac{\eta_{\ell}}{4\Delta y_{j}} \left[\sum_{k'=k-1}^{k} \sum_{i'=i-1}^{i} \psi_{g,\ell,k',j,i'} - \psi_{g,\ell,k',j-1,i'} \right] + \frac{\xi_{\ell}}{4\Delta z_{k}} \left[\sum_{j'=j-1}^{j} \sum_{i'=i-1}^{i} \psi_{g,\ell,k,j',i'} - \psi_{g,\ell,k-1,j',i'} \right] + \frac{\sigma_{g,k,j,i}}{8} \left[\sum_{k'=k-1}^{k} \sum_{j'=j-1}^{j} \sum_{i'=i-1}^{i} \psi_{g,\ell,k',j',i'} \right] = \frac{1}{k_{\text{eff}}} \frac{1}{8} \sum_{g'=1}^{G} \chi_{g'g} \nu \sigma_{f,g',k,j,i} \sum_{\ell'=1}^{L} w_{\ell'} \left[\sum_{k'=k-1}^{k} \sum_{j'=j-1}^{j} \sum_{i'=i-1}^{i} \psi_{g',\ell',k',j',i'} \right] + \frac{1}{8} \sum_{g'=1}^{G} \sigma_{s,g,g',k,j,i} \sum_{\ell'=1}^{L} w_{\ell'} \left[\sum_{k'=k-1}^{k} \sum_{j'=j-1}^{j} \sum_{i'=i-1}^{i} \psi_{g',\ell',k',j',i'} \right], \quad (2.4)$$

and

$$\frac{1}{8} \frac{\alpha}{v_g} \left[\sum_{k'=k-1}^{k} \sum_{j'=j-1}^{j} \sum_{i'=i-1}^{i} \psi_{g,\ell,k',j',i'} \right] + \frac{\mu_{\ell}}{4\Delta x_i} \left[\sum_{k'=k-1}^{k} \sum_{j'=j-1}^{j} \psi_{g,\ell,k',j',i} - \psi_{g,\ell,k',j',i-1} \right] + \frac{\eta_{\ell}}{4\Delta y_j} \left[\sum_{k'=k-1}^{k} \sum_{i'=i-1}^{i} \psi_{g,\ell,k',j,i'} - \psi_{g,\ell,k',j-1,i'} \right] + \frac{\xi_{\ell}}{4\Delta z_k} \left[\sum_{j'=j-1}^{j} \sum_{i'=i-1}^{i} \psi_{g,\ell,k,j',i'} - \psi_{g,\ell,k-1,j',i'} \right] + \frac{\sigma_{g,k,j,i}}{8} \left[\sum_{k'=k-1}^{k} \sum_{j'=j-1}^{j} \sum_{i'=i-1}^{i} \psi_{g,\ell,k',j',i'} \right] = \frac{1}{8} \sum_{g'=1}^{G} \chi_{g'g} \nu \sigma_{f,g',k,j,i} \sum_{\ell'=1}^{L} w_{\ell'} \left[\sum_{k'=k-1}^{k} \sum_{j'=j-1}^{j} \sum_{i'=i-1}^{i} \psi_{g',\ell',k',j',i'} \right] + \frac{1}{8} \sum_{g'=1}^{G} \sigma_{s,g,g',k,j,i} \sum_{\ell'=1}^{L} w_{\ell'} \left[\sum_{k'=k-1}^{k} \sum_{j'=j-1}^{j} \sum_{i'=i-1}^{i} \psi_{g',\ell',k',j',i'} \right], \quad (2.5)$$

for $g=1,\ldots,G,\ i=1,\ldots,M,\ j=1,\ldots,J,\ k=1,\ldots,K,$ and $\ell=1,\ldots,L.$ In equations (2.4) and (2.5), $\sigma_g,\,\sigma_{s,g,g'},\,\nu\sigma_{f,g}$, and v_g , the total, scattering, and fission cross sections and the velocity for energy group g, are assumed to be constant on the cell $(x_{i-1} < x < x_i, y_{j-1} < y < y_j, z_{k-1} < z < z_k)$ (see Appendix A). We denote these values on each cell by $\sigma_{g,k,j,i},\,\sigma_{s,g,g',k,j,i},\,\nu\sigma_{f,g,k,j,i}$, and v_g .

2.1.5. Matrix formulation and the fixed-point iterative scheme

We use a matrix formulation similar to that of Refs. [9] and [44] to rewrite equations (2.4) and (2.5) in a more compact way:

$$\mathbf{H}\Psi = \left[\mathbf{S} + \frac{1}{k_{\text{eff}}}\mathbf{F}\right]\Psi,\tag{2.6}$$

and

$$\left[\alpha \mathbf{V}^{-1} + \mathbf{H}\right] \Psi = \left[\mathbf{S} + \mathbf{F}\right] \Psi. \tag{2.7}$$

Equations (2.6) and (2.7) are linear equations with $G \times L \times K \times J \times M$ unknowns for Ψ . The matrix operators, \mathbf{H} , \mathbf{S} , \mathbf{F} , and \mathbf{V} are constructed as Kronecker products of various smaller matrices that couple spatial, angular, and energy angular flux unknowns.

Starting from random values for $\Psi^{(0)}$ and $k^{(1)}$, we solve the k-effective problem (2.6) through the iterative process for $\tau \geq 1$:

$$\Psi^{(\tau+1)} = \mathbf{H}^{-1} \left[\mathbf{S} + \frac{1}{k_{\text{eff}}^{(\tau)}} \mathbf{F} \right] \Psi^{(\tau)},$$

$$k_{\text{eff}}^{(\tau+1)} = k_{\text{eff}}^{(\tau)} \frac{\sum \mathbf{F} \Psi^{(\tau+1)}}{\sum \mathbf{F} \Psi^{(\tau)}}.$$
(2.8)

Starting from random values for $\Psi^{(0)}$ and setting $\alpha^{(0)} = 0$, we solve for $k_{\text{eff}}^{(0)}$. We then set $\alpha^{(1)} = 0.01$ and solve for $k_{\text{eff}}^{(1)}$. Continuing this process we solve problem (2.7) through the iterative process for $\tau \geq 1$:

$$\begin{split} \left[\alpha^{(0)}\mathbf{V}^{-1} + \mathbf{H}\right]\Psi^{(0)} &= \left[\mathbf{S} + \frac{1}{k_{\mathrm{eff}}^{(0)}}\mathbf{F}\right]\Psi^{(0)} \leftarrow \text{solve this k-effective with } \alpha^{(0)}, \\ \left[\alpha^{(1)}\mathbf{V}^{-1} + \mathbf{H}\right]\Psi^{(1)} &= \left[\mathbf{S} + \frac{1}{k_{\mathrm{eff}}^{(1)}}\mathbf{F}\right]\Psi^{(1)} \leftarrow \text{solve this k-effective with } \alpha^{(1)}, \\ \alpha^{(\tau+1)} &= \alpha^{(\tau)} + \frac{1 - k_{\mathrm{eff}}^{(\tau-1)}}{(k_{\mathrm{eff}}^{(\tau)} - k_{\mathrm{eff}}^{(\tau-1)}) * (\alpha^{(\tau)} - \alpha^{(\tau-1)})}, \end{split}$$
(2.9)
$$\left[\alpha^{(\tau+1)}\mathbf{V}^{-1} + \mathbf{H}\right]\Psi^{(\tau+1)} &= \left[\mathbf{S} + \frac{1}{k_{\mathrm{eff}}^{(\tau+1)}}\mathbf{F}\right]\Psi^{(\tau+1)} \leftarrow \text{solve this k-effective with } \alpha^{(\tau+1)}. \end{split}$$

Since the matrices, \mathbf{H} , \mathbf{S} , \mathbf{F} , and \mathbf{V} , tend to be very large; in most cases, this iterative process is accomplished in PARTISN using a matrix-free method such as those described in Ref. [38].

2.2. Tensors and Tensor Networks

In our TT/QTT reformulation of the algorithms of Section 2.1, we will make extensive use of real, multidimensional tensors, i.e., multidimensional arrays of real numbers. We refer the reader to Refs. [33, 46] and Appendix B for more details about the notation and the concepts that we briefly review in this section.

2.2.1. Tensor network formats and tensor factorizations

The total number of elements N of a d-dimensional tensor, with $n_k = \mathcal{O}(n)$ elements in each dimension $k = 1, 2, \ldots d$ is exponential in d, i.e., $N = \mathcal{O}(n^d)$. Approximate tensor factorization compresses the full tensor with "acceptable" accuracy by using much fewer elements. Such a factorization is achieved through a multidimensional minimization that can include various constraints (sparsity, non-negativity, etc.) [33]. To define the tensor decompositions, we need the notion of tensor rank. A d-dimensional, rank-1 tensor is a tensor that can be represented as tensor product of d vectors, e.g., $\mathcal{G} = \mathbf{g}_1 \circ \mathbf{g}_2 \circ \ldots \circ \mathbf{g}_d$, or, componentwise, $\mathcal{G}(i_1, i_2, \ldots, i_d) = \mathbf{g}_1(i_1)\mathbf{g}_2(i_2)\ldots\mathbf{g}_d(i_d)$. The canonical rank of a tensor is the minimal number R of rank-1 tensors whose sum is equal to this tensor.

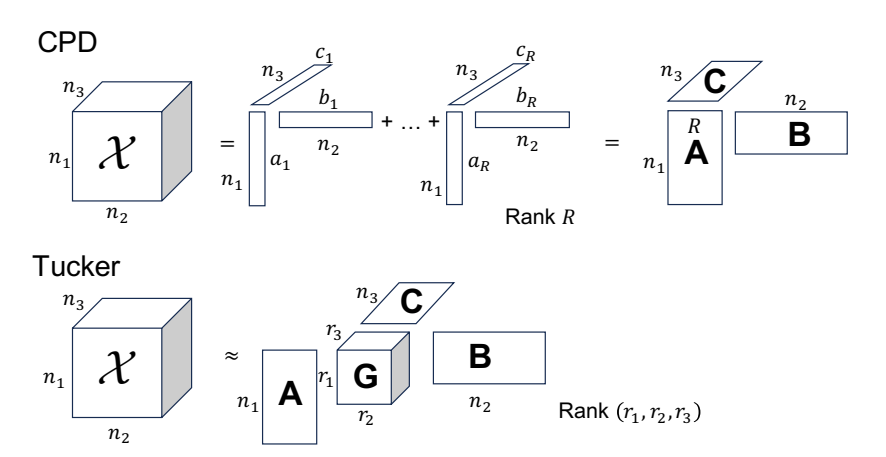


Figure 1: Top panel: Canonical Polyadic Decomposition (CPD) of a 3D tensor with size $N_\chi=n_1\times n_2\times n_3$ and rank R. Bottom panel: Tucker decomposition of a 3D tensor with size $N_\chi=n_1\times n_2\times n_3$ and multi-rank rank $r=[r_1,r_2,r_3]$.

As shown in Fig. 1 (top panel), the Canonical Polyadic Decomposition factorizes a d-dimensional tensor with rank R, presenting it as a sum of R rank-1, d-dimensional tensors, cf. [26]. This decomposition has the smallest possible number of elements, $\mathcal{O}(NdR)$. However, it requires knowledge of the canonical rank, whose computation is an NP-hard problem [27]. Therefore, the approximation of the full tensor by CPD, with its canonical rank R, can be inaccurate or ill-posed [16]. As shown in Fig. 1 (bottom panel), $Tucker\ decomposition$ factorizes a d-dimensional tensor by a product of d factor matrices and a small core tensor, \mathcal{G} with dimensions $r_1 \times r_2 \times \ldots \times r_d$, see Refs. [15, 54]. The set of the dimensions of the core tensor, \mathcal{G} , $\mathbf{r} := [r_1, r_2, \ldots, r_d]$, is called $Tucker\ multi-rank$. The number of Tucker decomposition elements, $\mathcal{O}(Ndr + r^d)$, remains exponential in d.

The Tensor Train (TT) format [46], seen as a linear chain of products of 3D tensors, is a very effective alternative to CPD and Tucker decomposition. Precisely, the TT approximation \mathcal{X}^{TT} of a d-dimensional tensor \mathcal{X} is a tensor with elements

$$\mathcal{X}^{TT}(i_1, i_2, \dots, i_d) = \sum_{\alpha_1 = 1}^{r_1} \dots \sum_{\alpha_{d-1} = 1}^{r_{d-1}} \mathcal{G}_1(1, i_1, \alpha_1) \mathcal{G}_2(\alpha_1, i_2, \alpha_2) \dots \mathcal{G}_d(\alpha_{d-1}, i_d, 1) + \varepsilon, \quad (2.10)$$

where the last term, ε , is a tensor with the same dimensions of \mathcal{X} representing the approximation error. Equivalently, we can also denote the TT format by the multiple matrix product

$$\mathcal{X}^{TT}(i_1, i_2, \dots, i_d) = \mathbf{G}_1(i_1)\mathbf{G}_2(i_2)\dots\mathbf{G}_d(i_d) + \varepsilon, \tag{2.11}$$

where each term $(\mathbf{G}_k(i_k))_{\alpha_{k-1},\alpha_k}$, $i_k = 1, 2, \dots, n_k$, $k = 1, 2, \dots, d$, is a matrix of size $r_{k-1} \times r_k$ (with the assumption that $r_0 = r_d = 1$). Therefore, the TT cores $\mathcal{G}_k(:, i_k,:)$ are a set of matrix slices $\mathbf{G}_k(i_k)$ that are labeled with the single index i_k . The entries of the integer array $\mathbf{r} = [r_1, \dots, r_{d-1}]$ are the TT ranks, and quantify the compression effectiveness. Since each TT core only depends on a single mode index of the full tensor \mathcal{X} , e.g., i_k , the TT format effectively embodies a discrete separation of variables [4]. When the TT ranks are relatively small with respect to the problem size, a TT-based approach is referred to as a low-rank approximation [5].

Assuming that $n_k = \mathcal{O}(n)$ and $r_k = \mathcal{O}(r)$ for some nonnegative integers n and r, and for all k = 1, 2, ..., d, the total number of elements that TT format stores is proportional to $\mathcal{O}(2nr + (d-2)nr^2)$, which is linear with the number of dimensions d. Fig. 2 illustrates how

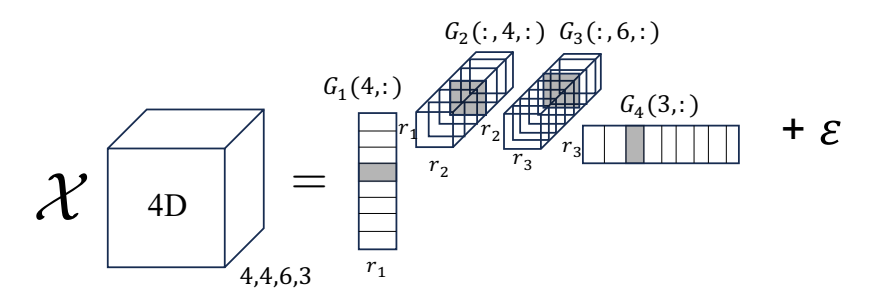


Figure 2: Approximate TT decomposition of a 4D tensor \mathcal{X} , with TT ranks $\mathbf{r} = [r_1, r_2, r_3, r_4]$, and approximation error ε , in accordance with Eq. (2.11). We compute the elements of full tensor \mathcal{X} as products of matrix slices and row and column vectors of the TT cores of \mathcal{X}^{TT} . For example, element $\mathcal{X}(4,4,6,3)$ is restored by the product of the fourth row vector from the first core \mathcal{G}_1 , the fourth and sixth matrix slices from the intermediate cores \mathcal{G}_2 and \mathcal{G}_3 , and the third column vector from the fourth and final core \mathcal{G}_4 . Column and row vectors and matrix slices are grey-shaded in the figure.

using the TT format, we can approximate a four-dimensional array with a certain error ε that we can suitably control. In fact, for a tensor admitting CPD with rank R and error η , there exists an approximate TT format factorization with ranks $r_k < R$ for each k = 1, 2, ..., d and $\varepsilon < \eta \sqrt{(d-1)}$ [48].

2.2.2. Grid functions in TT format and curse of dimensionality

How does the TT format break the curse of dimensionality when numerically solving high-dimensional PDEs? The numerical integration of a PDE requires representing grid functions and discrete operators in TT format. In Figure 3, a discretization of a 3D function with three points per dimension, resulting in a dense tensor (Fig. 3a-right), is also presented in a tensor network format (Fig. 3a-left). The depicted TT format equals a CPD format with rank R = 1. The tensor grid structure makes it possible to store the full-grid tensor with n = 3 entries per direction using only nd = 9 numbers. When expanded (Fig. 3a-right), the same amount of information requires storing $n^d = 27$ numbers. In the former situation, the complexity is proportional to d (linear in d), while, in the latter case, it is exponential in d. Therefore, we break the curse of dimensionality if we can perform all operations of the numerical algorithm solving the PDE through a tensor network format. Unfortunately, PDEs are usually discretized using the full tensor format, (Fig. 3b-left), which means that to break the curse of dimensionality, we must reformulate the PDE operators, functions, and algorithms on tensor grid functions using the approximate TT format (Fig. 3b-right) with a controlled error ε .

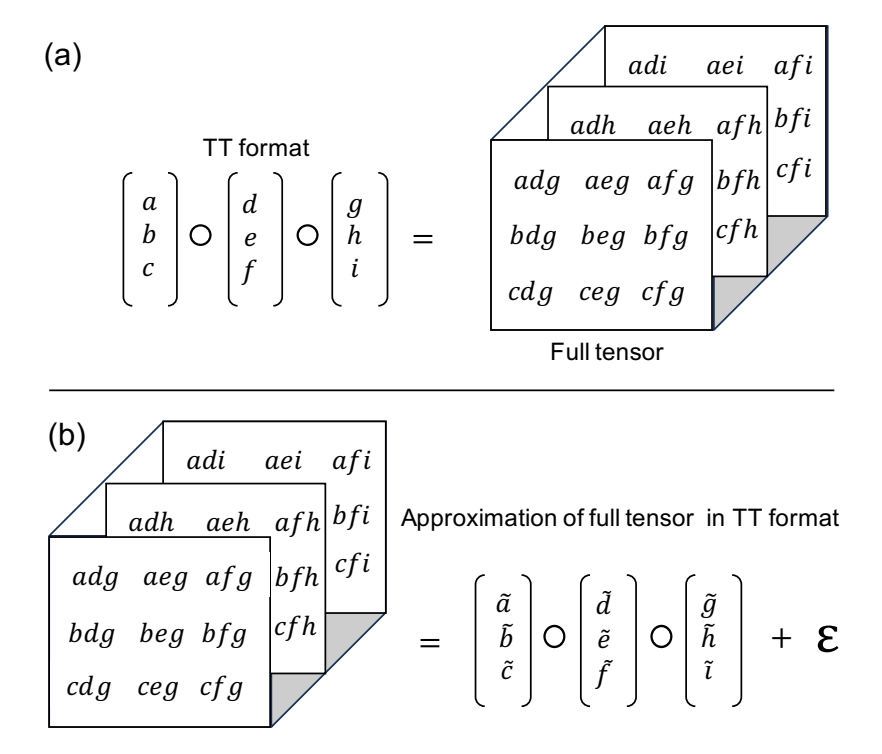


Figure 3: Breaking the curse of dimensionality: (A) The tensor product of three rank-1 vectors is a $3 \times 3 \times 3$ tensor, while (b) a $3 \times 3 \times 3$ tensor can be factorized into a rank-1 product of three vectors with a controlled error ε .

2.2.3. Differentiation, integration and interpolation operators of grid function in TT format

A critical aspect that enables the implementation of the TT format in numerical PDE methods is the ability to represent all discrete operators, such as differentiation, interpolation, integration, multiplication, etc. in TT format [3, 40]. For illustration, we consider d=4, and a real-valued, four-dimensional function $f(x_1, x_2, x_3, x_4)$, where each independent variable x_k , k=1,2,3,4, is defined over a proper domain range, e.g., \mathcal{D}_k , a bounded subinterval of \mathbb{R} . We introduce a four-dimensional, regular, Cartesian grid covering domain $\mathcal{D}=\mathcal{D}_1\times\mathcal{D}_2\times\mathcal{D}_3\times\mathcal{D}_4$ and having n_k nodes along the k-th direction. We let $\mathcal{F}=\left(\mathcal{F}(i_1,i_2,i_3,i_4)\right)$ denote the tensor that consists of the values of f sampled at the grid nodes indexed by (i_1,i_2,i_3,i_4) . We also let the tensor \mathcal{F} be approximated by tensor \mathcal{F}^{TT} in TT format with cores $\mathcal{G}_k(:,i_k:)$ as in (2.10) and approximation error ε . The tensor ε has the same dimensions and size as \mathcal{F} and \mathcal{G} and may include other approximation errors due to the numerical differentiation, integration, and interpolation and its value may be different at any instance. More details on TT format representation of differentiation, integration, and interpolation operators are given in Appendix B.2, Appendix B.3, and Appendix B.4, respectively.

2.2.4. Linear Operators in TT format.

A numerical discretization often transforms the unknown multivariate function into a very long vector of degrees of freedom and the operators acting linearly on this vector become very large, sparse matrices. A linear operator **A** acting on a vector **x** with size $N_{\mathbf{x}} = n_1 n_2 \dots n_d$, which collects the degrees of freedom of a PDE associated with the multidimensional grid nodes indexed by (i_1, i_2, \dots, i_d) , has a matrix representation with size $N_{\mathbf{A}} = N_{\mathbf{x}} \times N_{\mathbf{x}}$. Instead of

using a plain matrix-vector format, we retain the TT format for matrices representing linear operators (see, e.g., [46, Section 4.3] and [47]), which generalizes the TT format of (2.10) from "multi-dimensional vectors" to "multi-dimensional matrices". To this end, we first note that we can represent the degrees of freedom of a d-dimensional PDE by reshaping vector \mathbf{x} into a d-dimensional tensor, e.g., $\mathcal{X}(j_1,\ldots,j_d)$. Consistently, we can reshape operator \mathbf{A} into a "matrix" tensor, e.g., $\mathcal{A}((i_1,\ldots,i_d),(j_1,\ldots,j_d))$. Here, the mode index pair (i_k,j_k) is formed by the "(input, output)" mode indices such that the application of \mathcal{A} to \mathcal{X} , i.e., $\mathcal{A}\mathcal{X}$, transforms any input mode index j_k in $\mathcal{X}(\ldots,j_k,\ldots)$ into the output mode index i_k of $(\mathcal{A}\mathcal{X})(\ldots,i_k,\ldots)$, according to the formula

$$(\mathcal{A}\mathcal{X})(i_1, i_2, \dots, i_d) = \sum_{j_1=1}^{n_1} \sum_{j_2=1}^{n_2} \dots \sum_{j_d=1}^{n_d} \mathcal{A}(i_1, i_2, \dots, i_d, j_1, \dots, j_d) \mathcal{X}(j_1, \dots, j_d).$$

To pursue this strategy further, we permute the mode indices of A to pair together the input/output indices as in

$$A(i_1, i_2, \dots, i_d, j_1, j_2, \dots, j_d) \xrightarrow{\text{permute}} A((i_1, j_1), (i_2, j_2), \dots, (i_d, j_d)).$$
 (2.12)

(We added the inner parenthesis to outline the index pairs). The benefit of such permutation is that it helps separate/decompose the dimensions whenever a "matrix" operator act on a single dimension independently of the other dimensions. The component-wise TT-format expression of the index-permuted, linear operator \mathcal{A}^{TT} reads as:

$$\mathcal{A}^{TT}(i_1, j_1, i_2, j_2, \dots, i_d, j_d) = \sum_{\alpha_1, \alpha_2, \dots, \alpha_{d-1} = 1}^{r_1, r_2, \dots, r_{d-1}} \mathcal{A}_1(1, (i_1, j_1), \alpha_1) \mathcal{A}_2(\alpha_1, (i_2, j_2), \alpha_2) \dots$$

$$\dots \mathcal{A}_d(\alpha_{d-1}, (i_d, j_d), 1), \quad (2.13)$$

where we make use of the 4D real cores $A_k = (A_k(\alpha_{k-1}, (i_k, j_k), \alpha_k) \in \mathbb{R}^{r_{k-1} \times m_k \times n_k \times r_k}$, with $r_0 = r_d = 1$, and $k = 1, 2, \dots, d$. In (2.13), we enclosed the space indices in parenthesis, i.e., (i_k, j_k) , to outline them. Analogously to (2.10) and (2.11), we can reformulate (2.13) as the multiple matrix product

$$\mathcal{A}^{TT}(i_1, j_1, i_2, j_2, \dots, i_d, j_d) = \mathbf{A}_1(i_1, j_1) \mathbf{A}_2(i_2, j_2) \dots \mathbf{A}_d(i_d, j_d).$$
 (2.14)

Equation (2.14) is equivalent to (2.13) since each 4D core $A_k(\alpha_{k-1},(i_k,j_k),\alpha_k)$ can be seen as

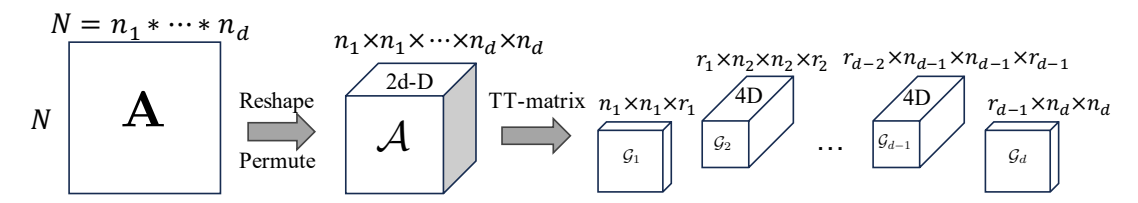


Figure 4: Representation of a linear operator in the TT-matrix format. First, we reshape the operation matrix \mathbf{A} into a 2d dimensional tensor \mathcal{A} and permute its indices. Then, we factorize the tensor in the tensor-train matrix format according to Eq. (2.13).

an $r_{k-1} \times r_k$ -sized, real matrix $(\mathbf{A}(i_k, j_k))_{\alpha_{k-1}, \alpha_k}$ in the indices α_{k-1} and α_k , where the index

pair (i_k, j_k) acts parametrically for $i_k = 1, 2, ..., m_k$, $j_k = 1, 2, ..., n_k$. Fig. 4 illustrates the steps needed to construct the TT-matrix representation of a linear operator.

We can further simplify the TT-matrix representations of \mathcal{A} in (2.13) and (2.14) and the action of tensor \mathcal{A} on tensor \mathcal{X} in TT formats if the internal ranks of \mathcal{A} are all equal to 1. In such a case, all summations in Eq. (2.13) reduce to a sequence of single matrix-matrix multiplications, and \mathcal{A} becomes the tensor product of d matrices:

$$\mathcal{A}^{TT} = \mathbf{A}_1 \circ \mathbf{A}_2 \circ \dots \circ \mathbf{A}_d. \tag{2.15}$$

We show below how this approach works through the discretization of the 3D Laplace differential operator on a cubic domain. In the 1D case, a finite difference discretization can be represented as a $n \times n$ -sized, banded, Toeplitz matrix $\mathbf{L_1}$. Assuming, for simplicity, that $n = n_1 = n_2 = n_3$, the $(n^3 \times n^3)$ -sized matrix $\mathbf{L_3}$ of the Laplace operator can be constructed as follows (see, e.g., [46, Section 3.1]):

$$L_3 = L_1 \otimes I_n \otimes I_n + I_n \otimes L_1 \otimes I_n + I_n \otimes I_n \otimes L_1$$

where $\mathbf{I_n}$ is the $n \times n$ identity matrix. It is clear that \mathbf{L}_3 can be considered as a reshaping of the 6D tensor \mathcal{L}_3 representing the Laplace differential operator in the multi-dimensional setting. Following the approach outlined above, we can directly construct tensor \mathcal{L}_3 by replacing the Kronecker product \otimes by the tensor product \circ , to obtain that

$$\mathcal{L}_3 = \mathbf{L}_1 \circ \mathbf{I_n} \circ \mathbf{I_n} + \mathbf{I_n} \circ \mathbf{L_1} \circ \mathbf{I_n} + \mathbf{I_n} \circ \mathbf{I_n} \circ \mathbf{L_1},$$

and we can represent each of these three rank-1 terms in TT format using Eq. (2.11). For example, the first term of the right-hand side has elements:

$$(\mathbf{L}_1 \circ \mathbf{I_n} \circ \mathbf{I_n})^{TT} (i_1, j_1, i_2, j_2, i_3, j_3) = \mathbf{L}_1 (1, i_1, j_1, 1) \mathbf{I_n} (1, i_2, j_2, 1) \mathbf{I_n} (1, i_3, j_3, 1).$$

Finally, we note that this process yields tensor \mathcal{L}_3 in TT format since the sum of tensors in TT format is itself a tensor in TT format, see, e.g., [46], although a rank reduction step could be necessary [46]. Importantly, as we will show later, the discrete differential operators of the NTEs possess similar structures as the high-dimensional Laplace operator.

2.2.5. Boundary Conditions

In general, incorporating boundary conditions into a discretization scheme involves modifying some entries of the discrete operators to account for the prescribed boundary conditions. By separating the variables, the TT format allows us to treat each dimension independently, making it easier to handle boundary conditions. For example, the boundary conditions for the dimension x_2 can be embedded into the differentiation matrix, e.g., **Diff** (see Appendix B, Eq. (B.6)), which, then, is applied to the second core \mathcal{G}_2 as shown in Fig 5.

2.2.6. Quantized Tensor Train (QTT) Format

TT format is very effective for the compression of high-dimensional tensors. However, for large low-dimensional objects, such as vectors, matrices, and tensors, the Quantized Tensor Train format [31] is even more effective. Specifically, we can reshape large vectors and matrices into high-dimensional tensors with a small number of elements in each dimension, and subsequently decompose these tensors in the TT format.

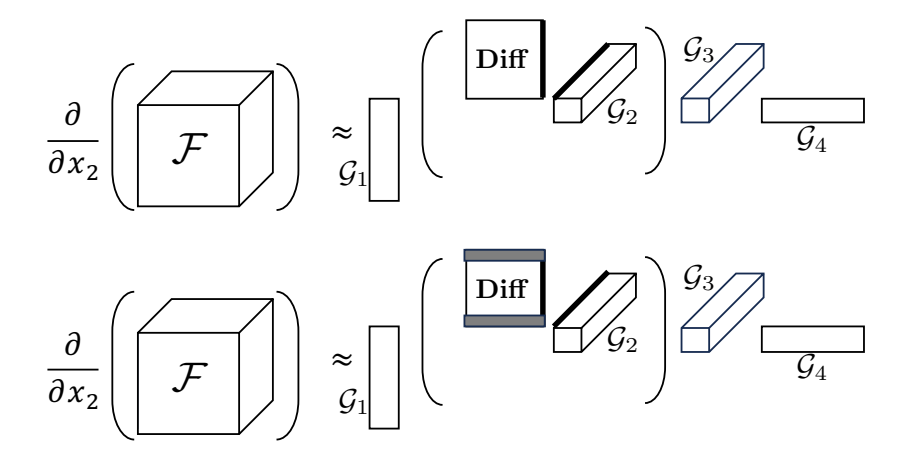


Figure 5: Top panel: Computing derivative with respect to x_2 in TT format by only applying the operation matrix **Diff** on the mode (**bold**) dimension of the second core \mathcal{G}_2 . Bottom panel: Boundary conditions (grey) for the second dimension x_2 are incorporated into the matrix operation of differentiation, **Diff**.

2.2.7. Quantized Tensor Train representation of vectors

Consider the vector $\mathbf{x} \in \mathbb{R}^{2^n}$. We first reshape \mathbf{x} to a $2 \times 2 \times \ldots \times 2$ -sized n-dimensional tensor, e.g., $\mathcal{X} \in \mathbb{R}^{2 \times \ldots \times 2}$. Then, we decompose this tensor in TT format, and called this TT tensor representation the QTT format; see, e.g., Fig 6. The QTT format exploits the fact that high-dimensional tensors, as well as extra-large matrices that correspond to physics [56] often possess low-rank structures, meaning that the corresponding quantized tensor can be well approximated by a combination of low-rank tensor cores. QTT is an example of the so-called "blessing of dimensionality" [55], which is used to describe the favorable properties that emerge when dealing with high-dimensional data. The "blessing of dimensionality" of QTT manifests itself in the form of improved compression efficiency.

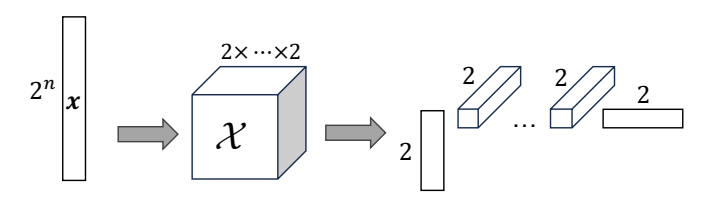


Figure 6: QTT format of a vector \mathbf{x} . The vector is first reshaped into an *n*-dimensional tensor \mathcal{X} of size $2 \times \cdots \times 2$, and then the TT format of that tensor is computed.

2.2.8. Quantized Tensor Train representation of linear operators

Let $\mathbf{A} \in \mathbb{R}^{2^n \times 2^n}$ be the matrix form of a linear operator. Converting this to a QTT matrix is a special case of the TT-matrix format for linear operators, described in Section 2.2.3, where all the dimensions sizes are 2. First, we reshape matrix \mathbf{A} into a 2n-dimensional tensor \mathcal{A} of size $2 \times 2 \times \ldots \times 2$ (n times). Then, the dimensions of \mathcal{A} is permuted as follows:

$$A(i_1, i_2, \dots, i_n, j_1, \dots, j_n) = A((i_1, j_1), (i_2, j_2), \dots; (i_n, j_n)),$$

finally, we decompose this tensor using the TT-matrix format described in Eq. (2.13) as

$$\mathcal{A}^{QTT}((i_1, j_1), (i_2, j_2), \dots, (i_n, j_n)) = \sum_{\alpha_1, \dots, \alpha_{d-1} = 1}^{r_1, \dots, r_{d-1}} \mathcal{A}_1(1, i_1, j_1, \alpha_1) \mathcal{A}_2(\alpha_1, i_2, j_2, \alpha_2) \dots$$
$$\dots \mathcal{A}_n(\alpha_{n-1}, i_n, j_n, 1),$$

where the first and the final cores are the 3D tensors $\mathcal{A}_1 \in \mathbb{R}^{2 \times 2 \times r_1}$ and $\mathcal{A}_n \in \mathbb{R}^{r_{l_k-1} \times 2 \times 2}$, and each intermediate core is the 4D tensor $\mathcal{A}_m \in \mathbb{R}^{r_{m-1} \times 2 \times 2 \times r_m}$, $m = 2 \dots n-1$.

3. Results

3.1. Tensorization of Boltzmann Neutron Transport Equation

Numerically solving PDEs often leads to ultra-large linear algebra problems, such as, linear systems of equations, $\mathbf{A}\mathbf{x} = \mathbf{b}$, or generalized eigenvalue problems, $\mathbf{A}\mathbf{x} = \lambda \mathbf{B}\mathbf{x}$. To avoid the curse of dimensionality, we reformat all operators and vectors in TT format to achieve a computational complexity that grows linearly, rather than exponentially,

$$\begin{aligned} \mathbf{A}\mathbf{x} &= \mathbf{b} & \rightarrow \mathcal{A}^{TT}\mathcal{X}^{TT} &= \mathcal{B}^{TT}, \\ \mathbf{A}\mathbf{x} &= \lambda \mathbf{C}\mathbf{x} & \rightarrow \mathcal{A}^{TT}\mathcal{X}^{TT} &= \lambda \mathcal{C}^{TT}\mathcal{X}^{TT}. \end{aligned}$$

Notice that \mathcal{A}^{TT} and \mathcal{C}^{TT} are in TT-matrix format (see subsection 2.2.4), while \mathcal{X} and \mathcal{B} are in TT format.

If some of the TT cores of \mathcal{A}^{TT} or \mathcal{C}^{TT} possess special tensor structures, they can be further compressed. For example, if a TT core has a Toeplitz structure, we can compress it using QTT format, since Toeplitz matrices have low-rank QTT formats [29]. This is the case for the neutron transport problem we solve below. Therefore, to achieve higher compression, we further transform these large TT cores into QTT format, and then solve the mixed TT/QTT version of the problems with an appropriate TT optimization technique (see 3.4). To find the biggest eigenvalue of the NTE problem we redesign a fixed-point scheme to work with the QTT format.

Below, we outline the main steps of our method:

- Forming the full tensor equation: We form the discretization (that leads to linear system or generalized eigenvalue problem) with boundary conditions included in the discrete matricised form of the operators. To be able to apply the QTT format, we choose the number of nodes of the grid in each dimension to be a power of two.
- TT format: We transform all objects in the full tensor equation into TT format.
- QTT format: We transform the TT cores that possess low-rank QTT structures into QTT format to achieve higher compression.
- Solving the problem in QTT format: We apply the available TT solvers, or design a new one, to solve the tensorized equations and obtain the solutions in TT format.

Next, we show how to apply this general approach to solve the NTE.

3.2. BNTE in TT format

In this section, we solve the discretization schemes for k-effective (see Eq. (2.6)) and alphaeigenvalue criticality problems (see Eq. (2.7)) utilizing the TT/QTT format for BNTE. In the traditional discretization, the operators \mathbf{H} , \mathbf{S} , \mathbf{F} , and \mathbf{V}^{-1} are designed as matrices that operate on the vectorized solution Ψ . This choice has been made to leverage existing linear algebra solvers specifically tailored for matrices. However, since the operation matrices are required to be fully formed, the problem size is limited. When the required storage exceeds the available memory, the matrix-free approach is used. However, using a matrix-free implementation can only help reducing the memory usage but not the computational cost.

In our approach, we seek the compact TT format of the eigenvector Ψ and the operators acting on it. The eigenvector Ψ in its original form is a five-dimensional tensor with dimensions $G \times L \times K \times J \times M$. Correspondingly, each operator acting on Ψ can be represented as a tendimensional tensor with dimensions $(G \times G) \times (L \times L) \times (K \times K) \times (J \times J) \times (M \times M)$. We denote these tensor operators as \mathcal{H} , \mathcal{S} , \mathcal{F} , and \mathcal{V}^{-1} , where $\mathcal{H} = \mathcal{H}_x + \mathcal{H}_y + \mathcal{H}_z + \mathcal{H}_\sigma$. Eqs. (3.1) below lists the operators that we need to construct in TT format and their terms, which are given in Equations (2.4) and (2.5):

$$\frac{\mu_{\ell}}{4\Delta x_{i}} \left[\sum_{k'=k-1}^{k} \sum_{j'=j-1}^{j} \psi_{g,\ell,k',j',i} - \psi_{g,\ell,k',j',i-1} \right] \rightarrow \mathcal{H}_{x}\Psi,$$

$$\frac{\eta_{\ell}}{4\Delta y_{j}} \left[\sum_{k'=k-1}^{k} \sum_{i'=i-1}^{i} \psi_{g,\ell,k',j,i'} - \psi_{g,\ell,k',j-1,i'} \right] \rightarrow \mathcal{H}_{y}\Psi,$$

$$\frac{\xi_{\ell}}{4\Delta z_{k}} \left[\sum_{j'=j-1}^{j} \sum_{i'=i-1}^{i} \psi_{g,\ell,k,j',i'} - \psi_{g,\ell,k-1,j',i'} \right] \rightarrow \mathcal{H}_{z}\Psi,$$

$$\frac{\sigma_{g,k,j,i}}{8} \left[\sum_{k'=k-1}^{k} \sum_{j'=j-1}^{j} \sum_{i'=i-1}^{i} \psi_{g,\ell,k',j',i'} \right] \rightarrow \mathcal{H}_{\sigma}\Psi,$$

$$\frac{1}{k_{\text{eff}}} \frac{1}{8} \sum_{g'=1}^{G} \chi_{g'g} \nu \sigma_{f,g',k,j,i} \sum_{\ell'=1}^{L} w_{\ell'} \left[\sum_{k'=k-1}^{k} \sum_{j'=j-1}^{j} \sum_{i'=i-1}^{i} \psi_{g',\ell',k',j',i'} \right] \rightarrow \mathcal{S}\Psi,$$

$$\frac{1}{8} \sum_{g'=1}^{G} \sigma_{s,g,g',k,j,i} \sum_{\ell'=1}^{L} w_{\ell'} \left[\sum_{k'=k-1}^{k} \sum_{j'=j-1}^{j} \sum_{i'=i-1}^{i} \psi_{g',\ell',k',j',i'} \right] \rightarrow \mathcal{F}\Psi,$$

$$\frac{1}{8} \frac{\alpha}{v_{g}} \left[\sum_{k'=k-1}^{k} \sum_{j'=j-1}^{j} \sum_{i'=i-1}^{i} \psi_{g,\ell,k',j',i'} \right] \rightarrow \mathcal{V}^{-1}\Psi.$$

These operators possess specific algebraic structures and we can construct their TT-format representation explicitly through the equivalence described in Eq. (2.15). Each of these operators contains several univariate operators, i.e., operators acting on a single variable only. This fact allows us to formulate them as tensor products of matrices, which is equivalent to a TT format with TT rank equal to one. As an example, we describe below the algebraic structure of one of them, \mathcal{H}_x . By definition, operator \mathcal{H}_x explicitly depends on the five indices i, j, k, g, ℓ , which respectively discretize the dimensions x, y, z, the energy dimension, and the angular dimension. The dependence on i is through a first-order differentiation formula; the dependence on j and k is through an average; the dependence on ℓ is through a scaling factor, and the operator is independent of g. Specifically,

- Energy dimension: (index g) The operator \mathcal{H}_x does not make any change in the energy dimension. Therefore, we can represent the action of this part of \mathcal{H}_x as the identity matrix \mathbf{I}_G .
- Ordinate dimension: (index l) For each l, the operator \mathcal{H}_x multiply μ_l into the eigenvector Ψ . Therefore, we can represent this part of \mathcal{H}_x as a block diagonal matrix, \mathbf{Q}_{μ} , that contains all values of μ_l .
- Interpolation along z and y dimensions: (indices k and j) Along these dimensions, the operator performs an average of Ψ between any two adjacent nodes. This average is accomplished by the sums $\frac{1}{4} \sum_{k'=k-1}^{k} \sum_{j'=j-1}^{j}$. Therefore, we represent these parts of \mathcal{H}_x by two interpolation matrices, \mathbf{Ip}_x and \mathbf{Ip}_y .
- Differentiation along x dimension: (index i) This part of the operator \mathcal{H}_x performs a differentiation along x. Therefore, we represent this part of \mathcal{H}_x through the differentiation matrix, **Diff**. The boundary condition for the x dimension dependents on whether μ_l is positive or negative, which requires a specific incorporation in the differentiation matrix, cf. Figure 7.

The remaining operators may depend differently on these indices, but the way we treat them is similar. In all cases we base their TT/QTT discretization on the tensor operations discussed in Section 2.2.

This is the key observation that allow us to directly construct the BNTE operators in TT format as tensor products of univariate operators.

3.2.1. TT formats of all BNTE Left-Hand-Side (LHS) Operators

The BNTE interaction tensor \mathcal{H} that is on the LHS of the BNTE includes four operation tensors, cf. Eq. (2.4):

$$\mathcal{H} = \mathcal{H}_x + \mathcal{H}_y + \mathcal{H}_z + \mathcal{H}_\sigma.$$

Below we explicitly construct the operation matrices that are the TT cores in the TT format of the interaction operator \mathcal{H} .

Differentiation Matrices. The differentiation matrix, \mathbf{D}_x , is used to compute the finite difference along spatial dimensions x. The boundary conditions depend on the sign of the ordinate, see Eq. (A.4). In Fig. 7 we show an example of two boundary conditions for the 1D neutron transport equation, which has three variables, i.e. x, ordinate μ , and energy E. When μ is positive, the boundary condition BC1 is at i = M, when μ is negative, the boundary condition BC2 is at i = 0

For the positive ordinates μ_{ℓ} , the differentiation matrix acting on x dimension, \mathbf{D}_{x}^{+} is defined as:

$$\mathbf{D}_{x}^{+} \equiv \frac{1}{\Delta x} \begin{pmatrix} 1 \\ -1 & \ddots \\ & \ddots & \ddots \\ & & -1 & 1 \end{pmatrix} \in \mathbb{R}^{(M+1)\times(M+1)}, \qquad (3.2)$$

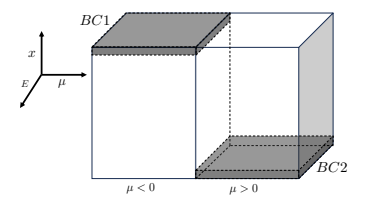


Figure 7: Boundary conditions BC1 and BC2 dependent on either μ 's values are positive or negative.

For the negative ordinates μ_{ℓ} , the differentiation matrix acting on x dimension, \mathbf{D}_{x}^{-} is defined as:

$$\mathbf{D}_{x}^{-} \equiv \frac{1}{\Delta x} \begin{pmatrix} -1 & 1 \\ & \ddots & \ddots \\ & & \ddots & 1 \\ & & & -1 \end{pmatrix} \in \mathbb{R}^{(M+1)\times(M+1)}. \tag{3.3}$$

In this way, we explicitly incorporate the boundary conditions in the differentiation matrices. The construction of the differentiation matrix in 3D for y and z, i.e. \mathbf{D}_y^+ , \mathbf{D}_y^- , \mathbf{D}_z^+ , and \mathbf{D}_z^- , is the same.

Interpolation Matrices. We use the interpolation matrix to approximate the BNTE solution, i.e., Ψ , in the centers of the grid cells based on vertex values. Similar to the differentiation matrix, the interpolation matrices incorporate the boundary conditions depending on the sign of the ordinate values. The interpolation matrices acting on the x dimension for $\mu_{\ell} < 0$, \mathbf{Ip}_{x}^{-} , and for $\mu_{\ell} > 0$, \mathbf{Ip}_{x}^{+} , are:

$$\mathbf{Ip}_{x}^{-} \equiv \frac{1}{2} \begin{pmatrix} 1 & 1 & & \\ & \ddots & \ddots & \\ & & \ddots & 1 \\ & & & 1 \end{pmatrix} \in \mathbb{R}^{(M+1)\times(M+1)}, \tag{3.4}$$

$$\mathbf{Ip}_{x}^{+} \equiv \frac{1}{2} \begin{pmatrix} 1 & & & \\ 1 & \ddots & & \\ & \ddots & \ddots & \\ & & 1 & 1 \end{pmatrix} \in \mathbb{R}^{(M+1)\times(M+1)}. \tag{3.5}$$

We also use interpolation matrices that do not include the boundaries:

$$\mathbf{Ip}_{x,noBC}^{-} \equiv \frac{1}{2} \begin{pmatrix} 1 & 1 & & \\ & \ddots & \ddots & \\ & & 1 & 1 \\ & & & 0 \end{pmatrix} \in \mathbb{R}^{(M+1)\times(M+1)}.$$
 (3.6)

$$\mathbf{Ip}_{x,noBC}^{+} \equiv \frac{1}{2} \begin{pmatrix} 0 \\ 1 & 1 \\ & \ddots & \ddots \\ & & 1 & 1 \end{pmatrix} \in \mathbb{R}^{(M+1)\times(M+1)}, \tag{3.7}$$

Angular Point Matrices. The angular matrices are used to multiply appropriate angular points to the correct terms on the left-hand-side of Eqs. (2.4) and (2.5). The dimensions of the angular matrices are $L \times L$. The angular matrices are 8-block diagonal matrices, in which each block corresponds to one of eight boundary conditions in (A.4). For each boundary condition, there are three angular matrices $\{\mathbf{Q}_{\mu}, \mathbf{Q}_{\eta}, \mathbf{Q}_{\xi}\}$, one for each angle μ , η , and ξ . For example, given the first boundary condition $\mu_{\ell} < 0$, $\eta_{\ell} < 0$, $\xi_{\ell} < 0$, the angular matrices are formed as follows:

$$\begin{cases}
\mathbf{Q}_{\mu} = \mathbf{C}_{1} \otimes \operatorname{diag}(\hat{\mu}_{-}) \\
\mathbf{Q}_{\eta} = \mathbf{C}_{1} \otimes \operatorname{diag}(\hat{\eta}_{-}) \\
\mathbf{Q}_{\xi} = \mathbf{C}_{1} \otimes \operatorname{diag}(\hat{\xi}_{-})
\end{cases}, \quad \mathbf{C}_{1} \equiv \begin{pmatrix} 1 \\ 0 \\ & \ddots \\ & & 0 \end{pmatrix} \in \mathbb{R}^{8 \times 8}, \tag{3.8}$$

where $\operatorname{diag}(\mu)$ is a square diagonal matrix with the elements of vector μ on the main diagonal; \mathbf{C}_i is a 8×8 matrix with $(\mathbf{C}_i)_{i,i}=1$, and zeros elsewhere; index i reflects the boundary condition. The quantities $\hat{\mu}_-, \hat{\eta}_-$, and $\hat{\xi}_-$ are defined in Section Appendix A.2.

Boundary Conditions. The $\mathcal{H}_j^{TT,bci}$ for the boundary condition bci, and for the variable $j \in \{x,y,z,\sigma\}$ can be explicitly built using the operation matrices defined above. For example, the $\mathcal{H}_j^{TT,bci=1}$, for the boundary condition 1 ($\mu_\ell < 0, \eta_\ell < 0, \xi_\ell < 0$) is defined as follows:

$$\mathcal{H}_{x}^{TT,1} = \mathbf{I}_{G} \circ \mathbf{Q}_{\mu} \circ \mathbf{I}\mathbf{p}_{z}^{-} \circ \mathbf{I}\mathbf{p}_{y}^{-} \circ \mathbf{D}_{x}^{-},$$

$$\mathcal{H}_{y}^{TT,1} = \mathbf{I}_{G} \circ \mathbf{Q}_{\eta} \circ \mathbf{I}\mathbf{p}_{z}^{-} \circ \mathbf{D}_{y}^{-} \circ \mathbf{I}\mathbf{p}_{x}^{-},$$

$$\mathcal{H}_{z}^{TT,1} = \mathbf{I}_{G} \circ \mathbf{Q}_{\xi} \circ \mathbf{D}_{z}^{-} \circ \mathbf{I}\mathbf{p}_{y}^{-} \circ \mathbf{I}\mathbf{p}_{x}^{-},$$

$$\mathcal{H}_{\sigma}^{TT,1} = \operatorname{diag}(\sigma) \circ (\mathbf{C}_{1} \otimes \mathbf{I}_{L/8}) \circ \mathbf{I}\mathbf{p}_{z}^{-} \circ \mathbf{I}\mathbf{p}_{y}^{-} \circ \mathbf{I}\mathbf{p}_{x}^{-}.$$

$$(3.9)$$

Other $\mathcal{H}_{i}^{TT,bci}$ are similarly constructed.

Velocity Tensor \mathcal{V}^{-1} . For solving the alpha-eigenvalue problem, we need the velocity tensor operator \mathcal{V}^{-1} , cf. Eq. (2.5). Similar to other operators, we construct the TT-format representation of \mathcal{V}^{-1} from its TT format for each boundary condition. For the boundary condition labeled by bci, the TT format representation of $(\mathcal{V}^{-1})^{TT,bci}$ is:

$$(\mathcal{V}^{-1})^{TT,bci} = \operatorname{diag}(1/\mathbf{v}) \circ (\mathbf{C}_1 \otimes \mathbf{I}_{L/8}) \circ \mathbf{I}\mathbf{p}_z^- \circ \mathbf{I}\mathbf{p}_y^- \circ \mathbf{I}\mathbf{p}_x^-.$$
 (3.10)

where \mathbf{v} is the velocity vector of all energy groups, and $1/\mathbf{v}$ is element-wise division.

3.2.2. TT formats of the BNTE Righ-Hand-Side (RHS) Operators

In view of Eq. (2.4), the RHS of the BNTE consists of two tensor operators, \mathcal{S} and \mathcal{F} . In the next two subsections, we explicitly construct the operation matrices that we use as TT cores in the TT format representation of these operators.

Integral Operator Matrix. Given $w \in \mathbb{R}^{L/8}$ is the weight vector from (A.1). The integral operator matrix for the first boundary condition is:

$$\mathbf{Intg}^1 = \mathbf{C}_1 \otimes (\mathbf{1}_{L/8} \otimes w)$$

where 1 is a vector of all ones.

Constructing \mathcal{F}^{TT} and \mathcal{S}^{TT} . Each operator $\mathcal{F}^{TT,bci}$ can be constructed using the above defined operation matrices. The $\mathcal{F}^{TT,1}$ matrix, for the first boundary condition, is shown below as an example:

$$\mathcal{F}^{TT,1} = \operatorname{diag}(\nu \sigma_f) \circ \mathbf{Intg}^1 \circ \mathbf{Ip}_{z,noBC}^- \circ \mathbf{Ip}_{y,noBC}^- \circ \mathbf{Ip}_{x,noBC}^-.$$
(3.11)

The operator $\mathcal{S}^{TT,1}$ can be similarly constructed as follows:

$$S^{TT,1} = \operatorname{diag}(\sigma_s) \circ \operatorname{Intg}^1 \circ \operatorname{Ip}_{z,noBC}^- \circ \operatorname{Ip}_{y,noBC}^- \circ \operatorname{Ip}_{x,noBC}^-$$
(3.12)

For the derivation of the remaining $\mathcal{F}^{TT,bci}$, $\mathcal{S}^{TT,bci}$, we refer to Appendix A. Then, $\mathcal{F}^{TT,bci}$ and $\mathcal{S}^{TT,bci}$ are used to construct \mathcal{F}^{TT} and \mathcal{S}^{TT} :

$$\mathcal{F}^{TT} = \sum_{bci=1}^{8} \mathcal{F}^{TT,bci}, \ \mathcal{S}^{TT} = \sum_{bci=1}^{8} \mathcal{S}^{TT,bci}.$$
 (3.13)

3.3. Transforming the BNTE Operators from TT to QTT format

Now that we have BNTE operators in TT format with TT rank one, we present a general strategy to reformat them in QTT format, using the fact that the operation matrices of the TT formatted tensors have a Toeplitz structure, [30]. To use the QTT format, the dimension sizes G, L, K, J, and M must be a power of two. It can be easily achieved by discretizing the full tensor by choosing the number of nodes in each dimension to be a power of two.

Given that all operators \mathcal{H}_x , \mathcal{H}_y , \mathcal{H}_z , \mathcal{H}_σ , \mathcal{S} , \mathcal{F} , and \mathcal{V}^{-1} possess similar TT structures, we describe the procedure to construct the QTT format for the generic operator $\mathcal{A} \in \{\mathcal{H}_x, \mathcal{H}_y, \mathcal{H}_z, \mathcal{H}_\sigma, \mathcal{S}, \mathcal{F}, \mathcal{V}^{-1}\}$.

For every boundary condition, indexed by $bci \in \{1, ..., 8\}$ (see Appendix and Eq. (A.4)), there exists a TT-matrix format representation of the generic discrete operator \mathcal{A}^{TT} , with TT rank one, which is specific to that boundary condition, hereafter denoted by $\mathcal{A}^{TT,bci}$,

$$\mathcal{A}^{TT,bci} = \mathbf{G}_1 \circ \mathbf{G}_2 \circ \mathbf{G}_3 \circ \mathbf{G}_4 \circ \mathbf{G}_5.$$

The next step is to convert the above operation matrices \mathbf{G}_k into their corresponding QTT-matrix formats. These matrices are of Toeplitz structures. The procedure to convert $\mathcal{A}^{TT,bci}$ to $\mathcal{A}^{QTT,bci}$ is described in the Algorithm 1.

```
Algorithm 1: Convert A^{TT} into A^{QTT}
```

```
Data: \mathcal{A}^{TT} = \mathbf{G}_1 \circ \mathbf{G}_2 \circ \mathbf{G}_3 \circ \mathbf{G}_4 \circ \mathbf{G}_5

Matrix \mathbf{G}_k has dimension of n_k \times n_k, where n_k = 2^{l_k}

Result: \mathcal{A}^{QTT}

1 for k = 1:5 do

2 Reshape \mathbf{G}_k to 2 \times \cdots \times 2 tensor \mathcal{G}_k

Permute \mathcal{G}_k(i_1, \dots, i_{l_k}, j_1, \dots, j_{l_k}) to \mathcal{G}_k(i_1, j_1, \dots, i_{l_k}, j_{l_k})

4 Compute \mathcal{G}_k's QTT-matrix format \mathcal{G}_k^{QTT} = g_1 g_2 \dots g_{l_k}

where the first core is 3D tensor g_1 \in \mathbb{R}^{2 \times 2 \times r_1}, the final core is a 3D tensor g_{l_k} \in \mathbb{R}^{r_{l_k-1} \times 2 \times 2} and each middle core, g_m, is a 4D tensor, g_m \in \mathbb{R}^{r_{m-1} \times 2 \times 2 \times r_m} for m = 2 \dots l_k - 1

5 \mathcal{A}^{QTT} = \mathcal{G}_1^{QTT} \mathcal{G}_2^{QTT} \mathcal{G}_3^{QTT} \mathcal{G}_4^{QTT} \mathcal{G}_5^{QTT}
```

Finally, the QTT format of the operator, \mathcal{A}^{QTT} , is the sum of all QTT format of that operator for each boundary condition:

$$\mathcal{A}^{QTT} = \sum_{bci=1}^{8} \mathcal{A}^{QTT,bci}.$$

3.3.1. QTT format of the Interaction Tensor \mathcal{H}^{QTT}

In Sec. 2.2.6 we described the general procedure to construct the QTT format for an operator. Importantly, we show above that the BNTE operators in TT format are tensor products of univariate operation matrices with specific algebraic structure. Therefore, next we define these matrices (or TT cores, \mathbf{G}_k) to construct each one of the NTE operators in the list $\{\mathcal{H}_x, \mathcal{H}_y, \mathcal{H}_z, \mathcal{H}_\sigma, \mathcal{S}, \mathcal{F}, \mathcal{V}^{-1}\}$ and transform them in QTT format exploiting their algebraic structure. We will start by describing how to construct the QTT format. Now we have all needed matrices to obtain the interaction operator \mathcal{H} in QTT format, which we will denote by, \mathcal{H}^{QTT} . Then using Algorithm 1, $\mathcal{H}_j^{TT,bci}$ is converted into the QTT format as $\mathcal{H}_j^{QTT,bci}$. Finally, the QTT format of the interaction tensor \mathcal{H} can be computed as:

$$\mathcal{H}^{QTT} = \sum_{j \in \{x, y, z, \sigma\}} \sum_{bci=1}^{8} \mathcal{H}_j^{QTT, bci}$$
(3.14)

3.3.2. QTT Format of Fission Operator \mathcal{F}^{QTT} and Scattering Operator \mathcal{S}^{QTT}

The QTT representations of fission operator \mathcal{F}^{QTT} and scattering operator \mathcal{S}^{QTT} are constructed in a similar fashion as \mathcal{H}^{QTT} . For each boundary condition, the component matrices are identified and converted to QTT format before being merged to finalized the QTT representation of the operator for that boundary condition.

3.3.3. Fixed-Point Algorithms in QTT format

We have completed constructing the QTT format of all operators needed to rewrite Eqn. (2.4) and (2.5) into QTT format. Next we will describe the TT solvers, and the fixed-point method [52] we utilize here, we use to solve these tensorized equations.

3.3.4. K-Effective Problem

A TT format analogous to Eq. (2.8) approximates the eigenvalue k_{eff} and the eigenvector Ψ^{QTT} in the QTT format for the following problem:

$$\mathcal{H}^{QTT}\Psi^{QTT} = \left[\mathcal{S}^{QTT} + \frac{1}{k_{\text{eff}}\mathcal{F}^{QTT}}\right]\Psi^{QTT}$$
(3.15)

Starting from random initial guesses for Ψ^{QTT} and k_{eff} , this equation can be solved using the following fixed point scheme:

$$\mathcal{B}^{QTT,(\tau)} = \left[\mathcal{S}^{QTT} + \frac{1}{k_{\text{eff}}^{(\tau)}} \mathcal{F}^{QTT} \right] \Psi^{QTT,(\tau)}$$

$$\mathcal{H}^{QTT} \Psi^{QTT,(\tau+1)} = \mathcal{B}^{QTT,(\tau)}$$

$$k_{\text{eff}}^{(\tau+1)} = k_{\text{eff}}^{(\tau)} \frac{\sum \mathcal{F}^{QTT} \Psi^{QTT,(\tau+1)}}{\sum \mathcal{F}^{QTT} \Psi^{QTT,(\tau)}},$$
(3.16)

where the last update rule comes from the traditional matrix-free approach, Eq. (3.16).

3.3.5. Alpha-eigenvalue Problem

Similarly, a TT format analog of Eq. (2.9) approximates the eigenvalue α and the eigenvector Ψ^{QTT} for the problem:

$$\left[\alpha \mathcal{V}^{-1,QTT} + \mathcal{H}^{QTT}\right] \Psi^{QTT} = \left[\mathcal{S}^{QTT} + \mathcal{F}^{QTT}\right] \Psi^{QTT}$$
(3.17)

Starting from random values for $\alpha^{(0)} = 0$, $\alpha^{(1)} = 0.01$, the alpha-eigenvalue problem in Eq. (2.5) can be solved as follows. First, we prepare the initial conditions by solving two k_{eff} problems, starting from random guesses for Ψ^{QTT} and k_{eff} and using updating rules given by Eq. (3.16):

$$\left[\alpha^{(0)}\mathcal{V}^{-1,QTT} + \mathcal{H}^{QTT}\right]\Psi^{QTT,(0)} = \left[\mathcal{S}^{QTT} + \frac{1}{k_{\text{eff}}^{(0)}}\mathcal{F}^{QTT}\right]\Psi^{QTT,(0)}
\left[\alpha^{(1)}\mathcal{V}^{-1,QTT} + \mathcal{H}^{QTT}\right]\Psi^{QTT,(1)} = \left[\mathcal{S}^{QTT} + \frac{1}{k_{\text{eff}}^{(1)}}\mathcal{F}^{QTT}\right]\Psi^{QTT,(1)},$$
(3.18)

which results in the needed four initial conditions: $\alpha^{(0)}=0$, $\alpha^{(1)}=0.01$, $k_{\rm eff}^{(0)}$, and $k_{\rm eff}^{(1)}$. Then using the update rule from traditional matrix-free approach, Eq. (2.9), we can calculate $\alpha^{(j+1)}$,

$$\alpha^{(\tau+1)} = \alpha^{j} + \frac{1 - k_{\text{eff}}^{(\tau-1)}}{(k_{\text{eff}}^{(\tau)} - k_{\text{eff}}^{(\tau-1)})(\alpha^{(\tau)} - \alpha^{(\tau-1)})}.$$
(3.19)

Second, we solve the next k_{eff} problem with the initial conditions, $\alpha^{(\tau+1)}$, and again using the updating rules given by Eq. (3.16) with random k_{eff} , Ψ^{QTT} :

$$\left[\alpha^{(\tau+1)}\mathcal{V}^{-1,QTT} + \mathcal{H}^{QTT}\right]\Psi^{QTT,(\tau+1)} = \left[\mathcal{S}^{QTT} + \frac{1}{k_{\text{eff}}^{(\tau+1)}}\mathcal{F}^{QTT}\right]\Psi^{QTT,(\tau+1)}$$
(3.20)

3.4. Tensor Optimization Techniques

In order to apply the update rules (described in the previous section) we need to be able to perform matrix/vector multiplications and solve systems of linear equations in QTT format. These tasked can be performed very efficiently in TT format, by manipulating a single TT core at the time, and using tensor optimization techniques, see [19, 28, 51].

These linear algebra problems first need to be formulated as optimization problems. For example, a linear system $\mathbf{A}\mathbf{x} = \mathbf{b}$ where \mathbf{x} , $\mathbf{b} \in \mathbb{R}^N$ and $\mathbf{A} \in \mathbb{R}^{N \times N}$, can be solved as the following minimization problem:

$$\mathbf{x} = \underset{\mathbf{y}}{\operatorname{argmin}} \mathcal{J}(\mathbf{y}) \text{ where } \mathcal{J}(\mathbf{y}) = \|\mathbf{A}\mathbf{y} - \mathbf{b}\|^2 = \mathbf{y}^T \mathbf{A}^T \mathbf{A} \mathbf{y} - 2\mathbf{b}^T \mathbf{A} \mathbf{y} + \mathbf{b}^T \mathbf{b}.$$
 (3.21)

Similarly, a matrix-vector multiplication **Ab** can be formulated as:

$$\mathbf{x} = \underset{\mathbf{y}}{\operatorname{argmin}} \mathcal{J}(\mathbf{y}) \text{ where } \mathcal{J}(\mathbf{y}) = \|\mathbf{A}\mathbf{b} - \mathbf{y}\|^2 = \mathbf{b}^T \mathbf{A}^T \mathbf{A} \mathbf{b} - 2\mathbf{y}^T \mathbf{A} \mathbf{b} + \mathbf{y}^T \mathbf{y}.$$
(3.22)

When the size of **A** and **b** are small enough, performing the matrix-vector multiplication **Ab** directly is straightforward. However, when their sizes are too big, and they possess low-rank TT structures, TT format is obviously a better option. In the TT format, there are an explicit and exact algorithm to compute the matrix-vector multiplication [46], but when compared to the tensor optimization techniques, they perform much slower. This is the reason we choose to perform the matrix-vector multiplication in TT format using the tensor optimization techniques.

For both problems in Eqs. (3.21) and (3.22), when **A**, **b**, and **y** are in TT format as $\hat{\mathcal{A}}^{TT}$, \mathcal{B}^{TT} , and \mathcal{Y}^{TT} , **x** is also in TT format, and:

$$\mathcal{X}^{TT} = \underset{\mathcal{Y}^{TT}}{\operatorname{argmin}} \mathcal{J}(\mathcal{Y}^{TT}) \tag{3.23}$$

Formulating the optimization problem in TT format enables the usage of algorithms that fix all but one TT core of \mathcal{Y}^{TT} , and turn the multilinear problem into a series of much smaller linear

problems for each TT core. These algorithms include Alternating Linear Scheme (ALS) [28], Two-Site Density Matrix Renormalization Group (DMRG) [51], or Alternating Minimal Energy (AMEn) [19], that can solve the minimization problem and find the optimal TT rank for it, without ever working with the full tensor. In general, these algorithms need as an input, \mathcal{A}^{TT} and \mathcal{B}^{TT} , as well as the initial guess for \mathcal{X}^{TT} (usually a random tensor with some TT rank), and the acceptable error, ε , for the solution. We have used amen_solve, and amen_mv in the MATLAB TT-Toolbox [45] to perform these calculations.

3.5. Numerical Experiments

3.5.1. A One-Dimensional Case Study

A one-dimensional slab problem was considered to verify the correctness of our TT-method and measure its performance. This problem is part of a criticality verification benchmark suite [53] and is exactly critical ($k_{\rm eff}=1,\,\alpha=0$). It consists of a plutonium-239 slab. The problem cross section data is shown in Table 1. The problem has energy one-group and the slab width is 3.707444~cm.

Material	ν	$\sigma_f \ (cm^{-1})$	$\sigma_s \ (cm^{-1})$	$\sigma_t \ (cm^{-1})$
Pu-239	3.24	0.081600	0.225216	0.32640

Table 1: Cross Section Data for 1D Benchmark Problem

We compared three approaches to solve this k-effective problem. The first approach uses a standard generalized eigen-solver (**GES**) to solve for the $k_{\rm eff}$. The second approach is the iterative solver described in equation 2.8applied to the full matricized format of the operators (**ISFM**), and the third approach is our TT/QTT iterative solver we build (**ISTT**). For the parameters, we set the number of spacial point to be 1024, and vary the number of ordinates $L \in \{2, 4, 6, 8, 16, 32\}$. These sizes are small enough to show how accurate the approximations are for both eigenvalues and eigenvectors. Moreover, given that we know the ground truth values for the $k_{\rm eff}$, we can show that by increasing L, the approximated eigenvalue should converge to the ground truth, ($k_{\rm eff} = 1$). For the iterative solvers and for the tensor train solver, the tolerance was set at 10^{-6} .

Figure 8 shows how well the eigenvalues and eigenvectors are approximated. Figure 8A shows that when increasing the number of ordinate L, the approximated eigenvalues from all three approaches converge to the ground truth value $k_{\rm eff}=1$, as expected. Figure 8B shows the difference in approximated eigenvalues between the approaches. The full matrices iterative solver can reach to the accuracy around 10^{-8} compared to the one from generalized eigenvalue solver. The difference in eigenvalue between the full matrices and the TT approaches is around 10^{-7} , which is below the TT truncated tolerance. Figure 8C shows the difference in the approximated eigenvectors. The full matrices and TT iterative approaches can reach to the accuracy around 10^{-4} compared to the eigenvector from generalized eigenvalue solver. The difference in eigenvector between the full grid and the TT approaches is around 10^{-8} , which is again below the TT truncated tolerance. Overall, this result shows that the TT approach produce very good approximations for both eigenvalues and eigenvectors.

We also measure the compression of the TT format using the compression ratio, which is defined as follows:

Compression ratio of
$$\Psi^{TT} = \frac{\# \text{ elements in TT format}}{\# \text{ elements in full grid tensor}}$$

Figure 9 shows the elapsed time of each solver, and the compression ratio of the approximated eigenvector in the TT format. Figure 9A shows that the TT approach takes significantly less time

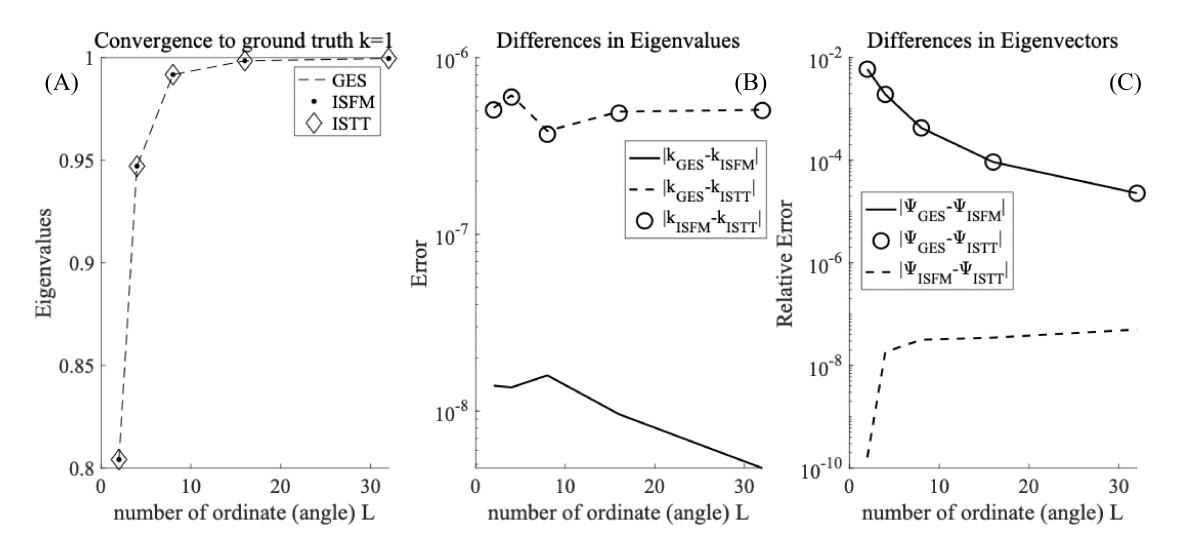


Figure 8: Comparison between three approaches to solve the k-effective problem. **GES** uses the generalized eigenvalue solver. **ISFM** is the iterative method for full matrix format of the operators. **ISTT** denotes our TT approach. $(Panel\ A)$ - Approximated eigenvalues converge to the ground truth value as the number of ordinate increases. $(Panel\ B)$ - Differences between approximated eigenvalues shows that the tensor train solver can approximate the eigenvalues with high accuracy. $(Panel\ C)$ - Differences between approximated eigenvectors shows that the eigenvector approximated by the tensor train solver is well matched with the ones from the full matrix iterative solver.

compared to the other solvers. For example, for the problem size with L=32, the TT approach is about 10 times faster than the others. Figure 9B shows the compression ratios around 10^{-2} , indicating that for these small problems, the TT format already gains about 2 orders of magnitude in term of the storage cost.

3.5.2. Benchmark problems

A variant of the critical assembly Jezebel was used to benchmark the tensor train approach for neutron transport. Jezebel was a tiny, nearly-spherical, nearly-bare (unreflected) experiment used from 1954-1955 to determine the critical mass of a homogeneous plutonium alloy [21]. For this paper, a cube variant of the assembly was considered. The cube has dimensions x=(0,10), y=(0,10), z=(0,10). The material is a mixture of plutonium-239, plutonium-240, plutonium-241, gallium-69, and gallium-71. The precise composition of the material is listed in Table 2. The material composition is given in atomic density, defined as the number of atoms per cubic centimeter of the material.

	Plutonium-239	Plutonium-240	Plutonium-241	Gallium-69	Gallium-71
Atomic Density $(\#/cm^3)$	3.7047e22	1.7512e21	1.1674e20	8.3603e20	5.3917e20

Table 2: Critical Benchmark Material Composition

The cube dimensions were chosen such that the problem was slightly supercritical. Discretization of the problem used three different spatial grid sizes with $N_x = N_y = N_z = N \in \{128, 256, 512\}$ grid points per spatial dimension. The 128 quadrature points on the unit sphere are generated when using an S_8 quadrature [57]. Lastly, 256 energy groups are used. For deterministic neutron transport calculations at Los Alamos National Laboratory, 30 energy groups are traditionally used since the cost of the computation scales linearly with the number of energy

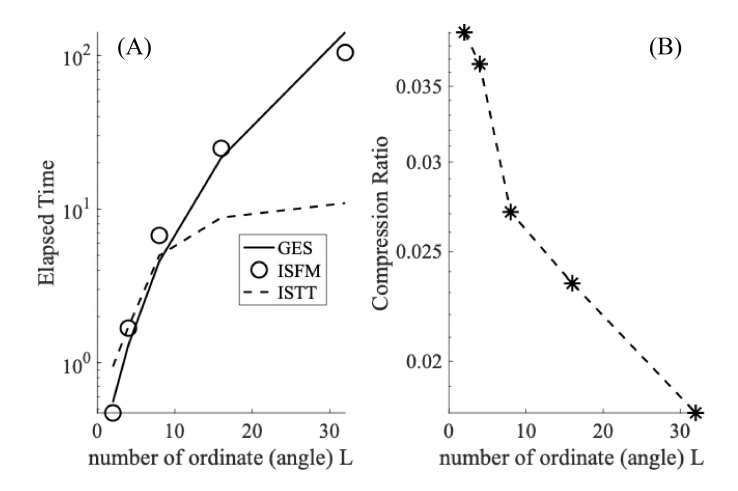


Figure 9: $(Panel\ A)$ - Comparison of the elapsed time between three approaches. The TT approach takes significantly less time compared to the others. At L=32, the TT approach is about 10 times faster $(Panel\ B)$ - Compression ratio of approximated eigenvectors in TT format shows that the TT approach already gains about 2 orders of magnitude in the storage cost.

groups. Using this discretization, the number of elements in the angular flux eigenvector Ψ is approximately 6.8×10^{10} elements (about 0.5 Terabytes (TB)) to 4.4×10^{12} elements (about 4.4 TB). Both the k-effective and alpha-eigenvalue problems were considered.

The TT/QTT approach applied to these problems is implemented using functions from the Oseledets's TT-Toolbox [45] and is benchmarked on a Linux system with a 10-core i9 processor and 32GB RAM.

3.5.3. Generation of Reference Values and PARTISN

Reference values for the k-effective and alpha-eigenvalues were generated using PARTISN (PARallel Time Dependent SN), the Los Alamos National Laboratory parallel time-dependent neutral particle SN transport code package [2]. The tensor train approach was compared to PARTISN. PARTISN numerically solves the neutron transport eigenvalue and source-driven problems in various geometries using a matrix-free solution method. The algorithm can briefly be described as follows: starting with an initial angular flux and eigenvalue, the scattering and fission sources are calculated for all cells, angles, and energy groups. Then, for all octants and energy groups, a known edge angular flux is used to "sweep" the problem by using known flux values to determine the neighboring cells' flux values. As mentioned earlier, unknown flux values are determined using the diamond differencing relationship. This solution of the angular flux iterate for all octants and energy groups is known as the "inner iteration." After obtaining the inner iteration fluxes, the scattering and fission sources are updated using the new angular flux, and the eigenvalue is updated. This is known as the "outer iteration." The process is repeated until the angular flux and eigenvalue converge to some tolerance. We note that the sweep of each energy group and octant is mathematically described as the solution of a lower triangular linear system using forward substitution. Throughout the algorithm, only the matrix-vector product of various quantities is required, allowing large problems to be solved without constructing the global linear system. We also note that the full neutron angular flux is not stored. Instead, the moments of the neutron angular flux are stored. In most cases, only the first moment of the neutron angular flux, the neutron scalar flux, is retained for eigenvalue problems. This further reduces the amount of memory required. Parallelization is achieved by either a spatial or energy

decomposition.

3.5.4. The k-effective Eigenvalue Problem

For these benchmark problems, the problem was decomposed over space in PARTISN. The performance of PARTISN is shown in Table 3. MPI ranks is the number of core that PARTISN used for the calculation on Snow, a LANL high-performance computing cluster.

Grid Size	Number of Iterations	Elapsed Time (seconds)	Time per Iter (seconds)	MPI Ranks	Scalar Flux Memory Storage (GB)	Eigenvalue
128	15	1131.323	75.42	72	4.29	1.0275823
256	15	5344.328	356.29	144	34.36	1.0276025
512	15	6061.987	404.13	1152	274.88	1.0276074

Table 3: Performance of PARTISN on 3D benchmark k-effective eigenvalue problem at different grid sizes. MPI ranks are the numbers of cores that PARTISN used for the calculation.

Next, we applied the TT/QTT approach to the benchmark problems. To approximate how much speed-up the tensor train approach has gained, we calculate the speed-up factor defined as follows:

$$speed-up \ factor = \frac{PARTISN \ elapsed \ time \times Number \ of \ cores \ used \ by \ PARTISN}{TT/QTT \ elapsed \ time \times Number \ of \ cores \ used \ by \ TT/QTT} \qquad (3.24)$$

Grid Size	Number of Iterations	Elapsed Time (seconds)	Speed-up factor	$\begin{array}{c} \text{full size of } \mathcal{H} \\ \text{(Zetabyte)} \end{array}$	Compression Ratio of \mathcal{H}	Ψ^{TT} Memory Storage (MB)	Eigenvalue Error
128	16	37.58	216.75	32	8.95e-18	1.03	6.53e-5
256	22	57.07	1348.5	2048	1.60e-19	0.98	3.26e-5
512	18	92.32	7564.4	131072	2.81e-21	1.15	3.44e-5

Table 4: Performance of Tensor Train approach on 3D benchmark k-effective eigenvalue problem at different grid

Table 4 shows that TT elapsed time is scaled at a slower rate when the grid size increases, increasing speed-up factors. For the largest problem at 512, the TT approach is about 7500 times faster than PARTISN. Next, the compression rate of \mathcal{H} shows the compression from yottabyte (YB) to megabyte (MB). The storage cost for Ψ in QTT format is only around 1MB, compared to the full tensor storage cost of about 0.5 TB. Finally, the TT approach has the accuracy of 10^{-5} in eigenvalue compared to the PARTISN reference solution.

We also want to point out that in PARTISN, only the scalar flux is possibly retained with the storage cost of hundreds of GBs, and it is impossible to store the operators whose sizes are YB. While in the TT/QTT format, both the operators and the eigenvectors can be compressed and stored with the cost of MB. This will enable possibilities to use other methods to solve for multiple eigen-pairs at once.

3.5.5. The Alpha-Eigenvalue Problem

Next, PARTISN was used to generate the reference alpha-eigenvalue for the comparison. The performance of PARTISN is shown in Table 5.

The performance of the TT approach on the benchmark alpha-eigenvalue problems is shown in Table 6. The result shows that the TT/QTT approach is significantly more efficient (about 4300 times faster for the largest problem). The increasing speed-up factor shows that the complexity of the TT approach scales at a lower rate compared to PARTISN. Moreover, the TT approach

Grid Size	Number of Iterations	Elapsed Time (seconds)	Time per Iter (seconds)	MPI Ranks	Scalar Flux Memory Storage (GB)	Eigenvalue
128	30	2475.821	82.53	72	4.29	9.2410746e-02
256	30	11637.28	378.91	144	34.36	9.2477425e-02
512	30	12783.57	426.12	1152	274.88	9.2493942e-02

Table 5: Performance of PARTISN on 3D benchmark alpha-eigenvalue problems at different grid sizes

Grid Size	Number of Iterations	Elapsed Time (seconds)	Speed-up factor	fullsize of H (Zetabyte)	Compression Ratio of H	Ψ^{TT} Memory Storage (MB)	Eigenvalue Error
128	3	64.06	278.22	32	8.95e-18	1.07	1.13e-4
256	8	131.69	1272.6	2048	1.60e-19	1.02	2.89e-5
512	7	336.56	4375.6	131072	2.81e-21	1.04	4.44e-5

Table 6: Performance of Tensor Train on 3D benchmark alpha-eigenvalue problem at different grid sizes

achieves the accuracy around 10^{-5} in approximating the alpha eigenvalues. The cost of storage is similar to the one from the k-effective eigenvalue problems, meaning while PARTISN needs about hundreds of GBs to store the scalar flux, the TT approach only uses about 1MB to store a whole eigenvector in TT format.

4. Conclusions

In this study, we utilize a low-rank tensor network method for solution of ultra large time-independent integro-differential Boltzmann Neutron Transport Equation. We introduce a mixed Tensor Train (TT)/Quantized Tensor Train (QTT) approach for numerical solution of 3D NTEs in Cartesian geometry. We discretize the NTE based on (a) diamond differencing; (b) multigroup-in-energy; (c) discrete ordinate collocation, which in realistic cases leads to extremely large generalized eigenvalue problems that requires matrix-free methods and large computer clusters. Further, we utilize this discretization and construct TT format of NTE followed by QTT formating of the large TT-cores, which enable a low-rank representation. In the final QTT format of NTE we solve the tensorized generalized eigenvalue problems using a fixed-point scheme and the TT-solver AMEn. Comparing the full grid solutions, calculated by PARTISN, with the solution of our TT/QTT method, we observed that the latter is exceptionally efficient in terms of computational time and memory usage, and significantly outperforms the full-grid version in computational efficiency and storage requirements, achieving an accuracy of 10^{-5} .

Acknowledgements

This work was supported by the Laboratory Directed Research and Development (LDRD) program of Los Alamos National Laboratory under the Grant 20230067DR, and in part by LANL Institutional Computing Program. Los Alamos National Laboratory is operated by Triad National Security, LLC, for the National Nuclear Security Administration of U.S. Department of Energy (Contract No. 89233218CNA000001).

References

 R. E. Alcouffe, R. S. Baker, J. A. Dahl, S. A. Turner, and R. Ward. Partisn: A Time-Dependent, Parallel Neutral Particle Transport Code System. Technical Report LA-UR-05-3925, Los Alamos National Laboratory, 2005.

- [2] R. E. Alcouffe et al. PARTISN: A time-dependent, parallel neutral particle transport code system. Technical Report LA-UR-17-29704, Los Alamos National Laboratory, 2022.
- [3] B. Alexandrov, G. Manzini, E. W. Skau, P. M. D. Truong, and R. G. Vuchov. Challenging the curse of dimensionality in multidimensional numerical integration by using a low-rank tensor-train format. *Mathematics*, 11(3):534, 2023.
- [4] M. Bachmayr, R. Schneider, and A. Uschmajew. Tensor networks and hierarchical tensors for the solution of high-dimensional partial differential equations. Foundations of Computational Mathematics, 16:1423–1472, 2016.
- [5] Markus Bachmayr. Low-rank tensor methods for partial differential equations. *Acta Numerica*, 32:1–121, 2023.
- [6] D. Balsara. Fast and accurate discrete ordinates methods for multidimensional radiative transfer. Part I, basic methods. *Journal of Quantitative Spectroscopy and Radiative Transfer*, 69(6):671–707, 2001.
- [7] G. I. Bell and S. Glasstone. Nuclear Reactor Theory. Van Nostrand Reinhold Company, New York, 1970.
- [8] R. Bellman. Dynamic programming. Science, 153(3731):34–37, 1966.
- [9] P. N. Brown. A linear algebraic development of diffusion synthetic acceleration for threedimensional transport equations. SIAM Journal on Numerical Analysis, 32(1):179–214, 1995.
- [10] B. G Carlson and K. D Lathrop. Transport Theory: The Method of Discrete Ordinates. Los Alamos Scientific Laboratory of the University of California, Los Alamos, New Mexico, 1965.
- [11] M. Chipot, W. Hackbusch, S. Sauter, and A. Veit. Numerical approximation of Poisson problems in long domains. *Vietnam Journal of Mathematics*, 50(2):375–393, 2022.
- [12] A. Cichocki. Tensor networks for big data analytics and large-scale optimization problems. arXiv preprint arXiv:1407.3124, 2014.
- [13] A. Cichocki, N. Lee, I. Oseledets, A.-H. Phan, Q. Zhao, D. P. Mandic, et al. Tensor networks for dimensionality reduction and large-scale optimization: Part 1 low-rank tensor decompositions. Foundations and Trends® in Machine Learning, 9(4-5):249–429, 2016.
- [14] A. Cichocki, A.-H. Phan, Q. Zhao, N. Lee, I. Oseledets, M. Sugiyama, D. P. Mandic, et al. Tensor networks for dimensionality reduction and large-scale optimization: Part 2 applications and future perspectives. Foundations and Trends® in Machine Learning, 9(6):431– 673, 2017.
- [15] L. De Lathauwer, B. De Moor, and J. Vandewalle. A multilinear singular value decomposition. SIAM journal on Matrix Analysis and Applications, 21(4):1253–1278, 2000.
- [16] V. De Silva and L.-H. Lim. Tensor rank and the ill-posedness of the best low-rank approximation problem. SIAM Journal on Matrix Analysis and Applications, 30(3):1084–1127, 2008.
- [17] D. E. Deutsch. Quantum computational networks. Proceedings of the royal society of London. A. mathematical and physical sciences, 425(1868):73–90, 1989.

- [18] S. V. Dolgov, B. N. Khoromskij, I. V. Oseledets, and D. V. Savostyanov. Computation of extreme eigenvalues in higher dimensions using block tensor train format. *Computer Physics Communications*, 185(4):1207–1216, 2014.
- [19] S. V. Dolgov and D. V. Savostyanov. Alternating minimal energy methods for linear systems in higher dimensions. SIAM Journal on Scientific Computing, 36(5):A2248-A2271, 2014.
- [20] J. J. Duderstadt and L. J. Hamilton. Nuclear Reactor Analysis. John Wiley & Sons, New York, 1976.
- [21] J. A. Favorite. Bare Sphere of Plutonium-239 Metal (4.5 at.% 240Pu, 1.02 wt.% Ga), PU-MET-FAST-001. International Handbook of Evaluated Criticality Safety Benchmark Experiments [DVD]/Nuclear Energy Agency, 2021.
- [22] R. P. Feynman and T. Hey. Quantum mechanical computers. In Feynman Lectures on Computation, pages 169–192. CRC Press, 2023.
- [23] P. Gelß, R. Klein, S. Matera, and B. Schmidt. Solving the time-independent Schrödinger equation for chains of coupled excitons and phonons using tensor trains. The Journal of Chemical Physics, 156(2), 2022.
- [24] Nikita Gourianov, Michael Lubasch, Sergey Dolgov, Quincy Y van den Berg, Hessam Babaee, Peyman Givi, Martin Kiffner, and Dieter Jaksch. A quantum-inspired approach to exploit turbulence structures. *Nature Computational Science*, 2(1):30–37, 2022.
- [25] W. Hackbusch. Tensor spaces and numerical tensor calculus, volume 42. Springer, 2012.
- [26] R. A Harshman. Determination and proof of minimum uniqueness conditions for PARAFAC1. *UCLA working papers in phonetics*, 22(111-117):3, 1972.
- [27] J. Håstad. Tensor rank is Np-complete. In Automata, Languages and Programming: 16th International Colloquium Stresa, Italy, July 11–15, 1989 Proceedings 16, pages 451–460. Springer, 1989.
- [28] S. Holtz, T. Rohwedder, and R. Schneider. The alternating linear scheme for tensor optimization in the tensor train format. *SIAM Journal on Scientific Computing*, 34(2):A683–A713, 2012.
- [29] V. A. Kazeev and B. N. Khoromskij. Low-rank explicit qtt representation of the Laplace operator and its inverse. SIAM journal on matrix analysis and applications, 33(3):742–758, 2012.
- [30] V. A. Kazeev, B. N. Khoromskij, and E. E. Tyrtyshnikov. Multilevel Toeplitz matrices generated by tensor-structured vectors and convolution with logarithmic complexity. *SIAM Journal on Scientific Computing*, 35(3):A1511–A1536, 2013.
- [31] B. N. Khoromskij. O (d log n)-quantics approximation of n-d tensors in high-dimensional numerical modeling. *Constructive Approximation*, 34:257–280, 2011.
- [32] B. N. Khoromskij. Tensor numerical methods in scientific computing, volume 19. Walter de Gruyter GmbH & Co KG, 2018.
- [33] T. G. Kolda and B. W. Bader. Tensor decompositions and applications. SIAM review, 51(3):455–500, 2009.

- [34] K. Kormann. A semi-lagrangian Vlasov solver in tensor train format. SIAM Journal on Scientific Computing, 37(4):B613–B632, 2015.
- [35] J. Kusch, B. Whewell, R. McClarren, and M. Frank. A low-rank power iteration scheme for neutron transport criticality problems. *Journal of Computational Physics*, 470:111587, 2022.
- [36] C. Kweyu, V. Khoromskaia, B. Khoromskij, M. Stein, and P. Benner. Solution decomposition for the nonlinear Poisson-Boltzmann equation using the range-separated tensor format. arXiv preprint arXiv:2109.14073, 2021.
- [37] E. E. Lewis and W. F. Miller. Computational methods of neutron transport. John Wiley and Sons, Inc., New York, NY, 1984.
- [38] E. E. Lewis and W. F. Miller. Computational Methods of Neutron Transport. John Wiley & Sons, New York, 1984.
- [39] G. Manzini, E. Skau, P. M. D. Truong, and R. Vangara. Nonnegative tensor-train low-rank approximations of the Smoluchowski coagulation equation. In *International Conference on Large-Scale Scientific Computing*, pages 342–350. Springer, 2021.
- [40] G Manzini, P. M. D. Truong, R Vuchkov, and B Alexandrov. The tensor-train mimetic finite difference method for three-dimensional Maxwell's wave propagation equations. *Mathematics and Computers in Simulation*, 210:615–639, 2023.
- [41] MATLAB. version 9.6 (R2019a). The MathWorks Inc., Natick, Massachusetts, 2019.
- [42] S. A. Matveev, D. A. Zheltkov, E. E. Tyrtyshnikov, and A. P. Smirnov. Tensor train versus Monte Carlo for the multicomponent Smoluchowski coagulation equation. *Journal* of Computational Physics, 316:164–179, 2016.
- [43] M. I. Ortega, R. N. Slaybaugh, P. N. Brown, T. S. Bailey, and B. Chang. A Rayleigh quotient method for criticality eigenvalue problems in neutron transport. *Annals of Nuclear Energy*, 138:107120, 2020.
- [44] M. I. Ortega, R. N. Slaybaugh, P. N. Brown, T. S. Bailey, and B. Chang. A Rayleigh quotient method for criticality eigenvalue problems in neutron transport. *Annals of Nuclear Energy*, 138:107120, 2020.
- [45] I. V. Oseledets. oseledet/TT-Toolbox. urlhttps://github.com/oseledets/TT-Toolbox.
- [46] I. V Oseledets. Tensor-train decomposition. SIAM Journal on Scientific Computing, 33(5):2295–2317, 2011.
- [47] I. V. Oseledets and S. V. Dolgov. Solution of linear systems and matrix inversion in the TT-format. SIAM Journal on Scientific Computing, 34(5):A2718–A2739, 2012.
- [48] Ivan Oseledets and Eugene Tyrtyshnikov. Tt-cross approximation for multidimensional arrays. *Linear Algebra and its Applications*, 432(1):70–88, 2010.
- [49] R. Penrose et al. Applications of negative dimensional tensors. *Combinatorial mathematics and its applications*, 1:221–244, 1971.
- [50] K. Ruymbeek, K. Meerbergen, and W. Michiels. Subspace method for multiparametereigenvalue problems based on tensor-train representations. *Numerical Linear Algebra with Applications*, 29(5):e2439, 2022.

- [51] D. Savostyanov and I. Oseledets. Fast adaptive interpolation of multi-dimensional arrays in tensor train format. In *The 2011 International Workshop on Multidimensional (nD) Systems*, pages 1–8. IEEE, 2011.
- [52] Yu A Shashkin. Fixed points, volume 2. Universities Press, 1991.
- [53] A. Sood, R. A. Forster, and D. K. Parsons. Analytical benchmark test set for criticality code verifiation. Progress in Nuclear Energy, 42(1):55–106, 2003.
- [54] L. R Tucker. Some mathematical notes on three-mode factor analysis. *Psychometrika*, 31(3):279–311, 1966.
- [55] E. Tyrtyshnikov. The blessing of dimensionality. Joint China and Russia Conference on Computational Mathematics Hong Kong Baptist University, 2010. https://www.math.hkbu.edu.hk/JCRCCM10/abstracts/Eugene.pdf (abstract).
- [56] M. Udell and A. Townsend. Why are big data matrices approximately low rank? SIAM Journal on Mathematics of Data Science, 1(1):144–160, 2019.
- [57] W. F. Walters. Use of the Chebyshev-Legendre quadrature set in discrete-ordinate codes. Technical Report LA-UR-87-3621, Los Alamos National Laboratory, 1987.
- [58] J. Wang. Matrix free methods for large scale optimization. PhD thesis, University of Washington, 2015.

Appendix A.

Appendix A.1. The Multigroup-in-Energy Approximation

The discretization in the energy variable must be detailed enough to capture the richness of neutron physics over a large energy domain. For example, neutron resonances of various isotopes are regions where the magnitude of a cross-section can vary rapidly over a small energy range. These nuclear physics effects must be carefully averaged in the energy discretization process to ensure reaction probabilities remain unchanged. To discretize the energy variable E, we use the *multigroup* approximation; see, e.g., [38]. We restrict the energy E to the finite interval E_{\min} , E_{\max} that we partition into E groups:

$$E_{\text{max}} = E_0 > E_1 > \dots > E_G = E_{\text{min}}.$$

Then, we average the eigenvalue equations (2.2) and (2.3), and we approximate the cross sections by a flux-weighted average over each energy group $E_g < E < E_{g-1}$. We denote the neutron angular flux at the discretized energy group g by ψ_g .

Appendix A.2. The Discrete-Ordinates Approximation

In nuclear reactors, the scattering of neutrons off materials like water or graphite can be highly anisotropic, requiring many discrete directions to resolve this behavior. Therefore, we must evaluates the transport equation along a set of discrete angular directions on the unit sphere that must be able to capture the possible anisotropy of the neutron angular flux. We discretize the angular variables using the discrete ordinates method [6] To discretize the angular variable,

we follow the process from [10] and consider a quadrature rule for approximating integrals on the unit sphere S^2 :

$$\int_{\mathcal{S}^2} d\hat{\Omega} \, \psi(\hat{\Omega}) \approx \sum_{\ell=1}^L w_\ell \psi(\hat{\Omega}_\ell) = \sum_{\ell=1}^L w_\ell \psi_\ell, \tag{A.1}$$

where $\psi_{\ell} = \psi(\hat{\Omega}_{\ell})$ is the neutron angular flux at direction ℓ and $\hat{\Omega}_{\ell} \equiv (\mu_{\ell}, \eta_{\ell}, \xi_{\ell})$, for ℓ ranging through 1 and $L = 2N^2$, N being the number of direction cosines. We assume that the quadrature weights w_{ℓ} are normalized so that $\sum_{\ell=1}^{L} w_{\ell} = 1$. In this work, We assume a square quadrature: a quadrature set where each axis has the same quadrature points forming a square grid of unique ordinates. Other types of quadrature can be considered if desired.

$$-1 < \mu_1 < \dots < \mu_{N/2} < 0 < \mu_{N/2+1} < \dots < \mu_N < 1, \mu_{N+1-n} = -\mu_n,$$

$$-1 < \eta_1 < \dots < \eta_{N/2} < 0 < \eta_{N/2+1} < \dots < \eta_N < 1, \eta_{N+1-n} = -\eta_n.$$

We note that since $\hat{\Omega}_{\ell} \in \mathcal{S}^2$ for all ℓ , ξ_{ℓ} and $\xi_{\ell} = \sqrt{1 - \mu_{\ell}^2 - \eta_{\ell}^2}$, is given by

$$\xi_{\ell} = \sqrt{1 - \mu_{\ell}^2 - \eta_{\ell}^2}$$

We collect the ordinates μ_{ℓ} in the arrays $\hat{\mu}_{-} = \left[\mu_{1}, \ldots, \mu_{L/2}\right]^{T}$ and $\hat{\mu}_{+} = \left[\mu_{L/2+1}, \ldots, \mu_{L}\right]^{T}$, and we similarly define the arrays $\hat{\eta}_{-}$, $\hat{\eta}_{+}$, $\hat{\xi}_{-}$, and $\hat{\xi}_{+}$. The ordering of the ordinates is arbitrary. The various combinations of ordinates specify faces of a three-dimensional surface and the ordering is chosen such that boundary conditions are simple to specify. For example, in reactor calculations, reactor fuel elements are symmetric and these lines of symmetry can be be used to reduce the size of the problem. In this case, the ordering of the ordinates prioritizes the vacuum boundary condition faces first and then the reflective faces. In this work we choose the ordinates ordering such that

since we are dealing exclusively with vacuum boundary conditions.

Appendix A.2.1. The Diamond-Difference Approximation

The space discretization must be of the order of the mean free path of a neutron before interacting, i.e., millimeters in a system like a nuclear reactor which measures in meters. We perform the discretization on the space independent variables x, y, and z using the diamond differencing method.

In the spatial dimension, we introduce a univariate grid partition over each problem dimension. We consider the grid stepsizes Δx_i , Δy_j , and Δz_k to partition the real, bounded intervals

 $[a_x, b_x]$, $[a_y, b_y]$, and $[a_z, b_z]$ into M, J, and K cells, respectively, so that

$$a_x \equiv x_0 < \dots < x_{i-1} < x_i < \dots < x_M \equiv b_x,$$

 $a_y \equiv y_0 < \dots < y_{j-1} < y_j < \dots < y_J \equiv b_y,$
 $a_z \equiv z_0 < \dots < z_{k-1} < z_k < \dots < z_K \equiv b_z,$

and $\Delta x_i = x_i - x_{i-1}$, $\Delta y_j = y_j - y_{j-1}$, and $\Delta z_k = z_k - z_{k-1}$. We refer to the grid nodes x_i, y_j , z_k as "edges" and we call "edge values" the corresponding function values.

Since cross-sections are constant in a cell, the cell-centered angular flux must be expressed in terms of edge angular flux values. The cell-centered angular flux is located at i - 1/2 and the diamond difference approximation [38] gives the cell-centered angular fluxes at the edges labeled by the index sets (k, j, i - 1/2), (k, j - 1/2, i), and (k - 1/2, j, i) as

$$\begin{split} \psi_{g,\ell,k,j,i-1/2} &= \frac{1}{2} \big(\psi_{g,\ell,k,j,i} + \psi_{g,\ell,k,j,i-1} \big), \\ \psi_{g,\ell,k,j-1/2,i} &= \frac{1}{2} \big(\psi_{g,\ell,k,j,i} + \psi_{g,\ell,k,j-1,i} \big), \\ \psi_{g,\ell,k-1/2,j,i} &= \frac{1}{2} \big(\psi_{g,\ell,k,j,i} + \psi_{g,\ell,k-1,j,i} \big). \end{split}$$

Appendix A.2.2. Discretization of the boundary conditions

Boundary conditions are defined for all faces of the three-dimensional problem. An incoming neutron angular flux can be imposed on a face of the problem. For example, an boundary flux on the top face of the three-dimensional cube would be expressed as

$$\psi_{g,\ell,K,J,M} = \Psi_{\text{top}} \quad \text{for } \mu_{\ell} < 0, \eta_{\ell} < 0, \xi_{\ell} < 0,$$
(A.3)

since we have defined $(\mu_{\ell} < 0, \eta_{\ell} < 0, \xi_{\ell} < 0)$ to be the inward direction, and K, J, M specifies that this incoming angular flux is for all cells in the top face of the problem. For eigenvalue problems, the boundary conditions are taken to be vacuum boundary conditions (no incoming angular flux) and the discretized boundary conditions for each face are given by

$$\psi_{g,\ell,K,J,M} = 0 \quad \text{for } \mu_{\ell} < 0, \eta_{\ell} < 0, \xi_{\ell} < 0
\psi_{g,\ell,K,J,0} = 0 \quad \text{for } \mu_{\ell} > 0, \eta_{\ell} < 0, \xi_{\ell} < 0
\psi_{g,\ell,K,0,M} = 0 \quad \text{for } \mu_{\ell} < 0, \eta_{\ell} > 0, \xi_{\ell} < 0
\psi_{g,\ell,K,0,0} = 0 \quad \text{for } \mu_{\ell} > 0, \eta_{\ell} > 0, \xi_{\ell} < 0
\psi_{g,\ell,0,J,M} = 0 \quad \text{for } \mu_{\ell} < 0, \eta_{\ell} < 0, \xi_{\ell} > 0
\psi_{g,\ell,0,J,0} = 0 \quad \text{for } \mu_{\ell} < 0, \eta_{\ell} < 0, \xi_{\ell} > 0
\psi_{g,\ell,0,0,M} = 0 \quad \text{for } \mu_{\ell} < 0, \eta_{\ell} > 0, \xi_{\ell} > 0
\psi_{g,\ell,0,0,0} = 0 \quad \text{for } \mu_{\ell} > 0, \eta_{\ell} > 0, \xi_{\ell} > 0
\psi_{g,\ell,0,0,0} = 0 \quad \text{for } \mu_{\ell} > 0, \eta_{\ell} > 0, \xi_{\ell} > 0.$$

The set of equations defined by Equations 2.4 and 2.5 have GLKJM unknowns and GLMK + GLJM + GLJK + GLM + GLJ + GLK + GL boundary equations.:

Appendix A.3. Matricization of the Discrete Neutron Transport Eigenvalue Equations

To write Equations 2.4 and 2.5 in matrix form, we define the angular flux vector for a single energy group g and direction ℓ as

$$\Psi_{g,\ell} \equiv \begin{pmatrix} \psi_{g,\ell,0} \\ \vdots \\ \psi_{g,\ell,K} \end{pmatrix} \in \mathbb{R}^{(K+1)(J+1)(M+1)},$$

$$\Psi_{g,\ell,k} \equiv \begin{pmatrix} \psi_{g,\ell,k,0} \\ \vdots \\ \psi_{g,\ell,k,J} \end{pmatrix} \in \mathbb{R}^{(J+1)(M+1)},$$

$$\Psi_{g,\ell,k,j} \equiv \begin{pmatrix} \psi_{g,\ell,k,j,0} \\ \vdots \\ \psi_{g,\ell,k,j,M} \end{pmatrix} \in \mathbb{R}^{(M+1)}. \quad (A.5)$$

The angular flux vector for an energy group g is defined as

$$\Psi_g \equiv \begin{pmatrix} \Psi_{g,1} \\ \vdots \\ \Psi_{g,L} \end{pmatrix} \in \mathbb{R}^{L(K+1)(J+1)(M+1)}. \tag{A.6}$$

The full angular flux vector is then defined as

$$\Psi \equiv \begin{pmatrix} \Psi_1 \\ \Psi_2 \\ \vdots \\ \Psi_G \end{pmatrix} \in \mathbb{R}^{GL(K+1)(J+1)(M+1)}. \tag{A.7}$$

Appendix A.3.1. Differencing and Interpolation Matrices

To write the matrix form of the diamond difference discretized derivative operators $\mu \partial/\partial x + \eta \partial/\partial y + \xi \partial/\partial z$, we define the matrices

$$\Delta x \equiv \operatorname{diag}(\Delta x_1, \dots, \Delta x_M) \in \mathbb{R}^{M \times M},$$

$$\Delta y \equiv \operatorname{diag}(\Delta y_1, \dots, \Delta y_J) \in \mathbb{R}^{J \times J},$$

$$\Delta z \equiv \operatorname{diag}(\Delta z_1, \dots, \Delta z_K) \in \mathbb{R}^{K \times K}.$$
(A.8)

The differencing matrix is defined as

$$D_x \equiv \begin{pmatrix} -1 & 1 \\ & \ddots & \ddots \\ & & -1 & 1 \end{pmatrix} \in \mathbb{R}^{M \times (M+1)}, \tag{A.9}$$

where the matrices D_y and D_z are defined similarly. Since each derivative term requires an average of cell-centered angular fluxes, we define the matrix S_x as

$$S_x = \frac{1}{2} \begin{pmatrix} 1 & 1 \\ & \ddots & \ddots \\ & & 1 & 1 \end{pmatrix} \in \mathbb{R}^{M \times (M+1)}, \tag{A.10}$$

where S_y and S_z are defined similarly. The matrices S_x , S_y , and S_z interpolate cell-centered vectors into zone-centered vectors by averaging the edge angular flux values.

Appendix A.3.2. Cell/Edge Transformation Matrices

We now define the matrices Z and Z_b as

$$Z \equiv \begin{pmatrix} I_{MJK} \\ 0 \end{pmatrix} \in \mathbb{R}^{(K+1)(J+1)(M+1)\times KJM}, \tag{A.11}$$

$$Z_b \equiv \begin{pmatrix} 0 \\ I_{(K+1)(J+1)(M+1)-KJM)} \end{pmatrix} \in \mathbb{R}^{(K+1)(J+1)(M+1)\times(K+1)(J+1)(M+1)-KJM}. \tag{A.12}$$

The matrices Z and Z_b transform cell-centered vectors to edge vectors and vice versa.

Appendix A.3.3. The Discrete Ordinates Matrices

We define the angular quadrature point matrices as

$$\hat{\mu} = \operatorname{diag}(\hat{\mu}_{-}, \hat{\mu}_{+}, \hat{\mu}_{-}, \hat{\mu}_{+}) \in \mathbb{R}^{L \times L},$$

$$\hat{\eta} = \operatorname{diag}(\hat{\eta}_{-}, \hat{\eta}_{-}, \hat{\eta}_{+}, \hat{\eta}_{+}) \in \mathbb{R}^{L \times L},$$

$$\hat{\xi} = \operatorname{diag}(\hat{\xi}_{-}, \hat{\xi}_{-}, \hat{\xi}_{+}, \hat{\xi}_{+}) \in \mathbb{R}^{L \times L}.$$
(A.13)

Discretized representations of the angular flux moment operators must be defined. These operators operate on zone-centered vectors and are easily seen to be given by $KJM \times LKJM$ size matrices

$$L_{n,m} \equiv (l_{n,m}W) \otimes I_{MJK},\tag{A.14}$$

where

$$l_{n,m} \equiv \left(Y_n^m(\hat{\Omega}_1), Y_n^m(\hat{\Omega}_2), \dots, Y_n^m(\hat{\Omega}_L) \right), \tag{A.15}$$

and

$$W \equiv \operatorname{diag}(w_1, w_2, \dots, w_L). \tag{A.16}$$

If the vector Ψ approximates $\psi(\mathbf{r}, \hat{\Omega})$, then $L_{n,m}\Psi$ approximates the $(n,m)^{\text{th}}$ moment of $\psi(\mathbf{r}, \hat{\Omega})$, $\phi_{n,m}(\mathbf{r})$. Similarly, we define $LMJK \times MJK$ size matrices

$$L_{n,m}^{+} \equiv l_{n,m}^{T} \otimes I_{MJK}. \tag{A.17}$$

If a vector Φ approximates $\phi(\mathbf{r})$, then $L_{n,m}^+\Phi$ approximates $Y_n^m(\hat{\Omega})\phi(\mathbf{r})$. We define the grouped matrices L_n and L_n^+ , where

$$L_n = \begin{pmatrix} L_{n,-n} \\ \vdots \\ L_{n,n} \end{pmatrix} \text{ and } L_n^+ = (L_{n,-n}^+, \dots, L_{n,n}^+,)$$
 (A.18)

and the further grouped block matrices

$$L^{N} = \begin{pmatrix} L_{0} \\ \vdots \\ L_{N} \end{pmatrix} \text{ and } L^{N,+} = \left(L_{0}^{+}, \dots, L_{N}^{+}\right), \tag{A.19}$$

where $N = N_s$, the number of terms in the scattering kernel. The scattering cross section in Eq. 2.2 is usually expanded in spherical harmonics up to some order $N_s[7]$. For this reason, it is assumed that the symmetric quadrature rule is such that the spherical harmonics of order N_s and less satisfy [9]

$$\sum_{\ell=1}^{L} Y_n^m(\hat{\Omega}_{\ell}) Y_{n'}^{m'}(\hat{\Omega}_{\ell}) = \delta_{n,n'} \delta_{m,m'}, \text{ for all } 0 \le n, n' \le N_s, |m| \le n, |m'| \le n'.$$
(A.20)

In this work, we assume all scattering is isotropic $(N_s = 0)$ for simplicity.

Appendix A.3.4. Matrix Representations of the Spatial Derivatives and Total Cross Section The matrix form representation of $\mu \partial/\partial x$, H_{μ} , can be written as

$$H_{\mu} = I_G \otimes \hat{\mu} \otimes Z(S_z \otimes S_y \otimes \Delta x^{-1} D_x), \tag{A.21}$$

where I_G is the identity matrix sized to the number of energy groups. The matrix H_{μ} is a square matrix with size $GL(K+1)(J+1)(M+1) \times GL(K+1)(J+1)(M+1)$. The other two derivative matrix terms, H_{η} and H_{ξ} can be written as

$$H_{\eta} = I_G \otimes \hat{\eta} \otimes Z(S_z \otimes \Delta y^{-1} D_y \otimes S_x), \tag{A.22}$$

and

$$H_{\xi} = I_G \otimes \hat{\xi} \otimes Z(\Delta z^{-1} D_z \otimes S_y \otimes S_x). \tag{A.23}$$

We define the total cross section matrices for energy group g over all cells as

$$\Sigma_g \equiv \operatorname{diag}(\sigma_{g,111}, \dots, \sigma_{g,KJM}) \in \mathbb{R}^{KJM \times KJM}.$$
(A.24)

The total cross section matrix for all energy groups is then

$$\Sigma = (I_G \otimes I_L \otimes Z) \bigg(I_L \otimes \operatorname{diag}(\Sigma_1, \dots, \Sigma_G) \bigg) \big(I_G \otimes I_L \otimes S \big)$$
(A.25)

where $S = S_z \otimes S_y \otimes S_x$.

To apply the boundary conditions shown in Eq. A.4, we define the matrices E_{kji} that pick out the correct elements of Ψ for some $\hat{\Omega}_{\ell}$ as done in [9]. There are eight different E_{kji} matrices in three-dimensions with k=0 or K, j=0 or J, and i=0 or M. For vacuum boundary conditions, we have

$$E_{kii}\Psi = 0. (A.26)$$

For ordinate $\hat{\Omega}_{\ell} > 0$ $(\mu_{\ell}, \eta_{\ell}, \xi_{\ell} > 0)$, the boundary matrix E_{000} is

$$E_{000} = \begin{pmatrix} e_{0K}^T \otimes I_{J+1} \otimes I_{M+1} \\ (0, I_K) \otimes e_{0J}^T \otimes I_{M+1} \\ (0, I_K) \otimes (0, I_J) \otimes e_{0M}^T \end{pmatrix}, \tag{A.27}$$

where e_{0M} is the basis vector sized M+1 with one as the first element and zero elsewhere. The other basic vectors are defined similarly. The boundary condition matrix B is then defined as

$$B = (I_G \otimes I_L \otimes Z_b) \bigg(I_G \otimes \operatorname{diag}(E_{KJM}, E_{KJM}, \dots, E_{000}, E_{000}) \bigg), \tag{A.28}$$

where the ordering of the matrices E_{kji} is determined by the signs of the quadrature points $(\mu_{\ell}, \eta_{\ell}, \xi_{\ell})$.

Appendix A.3.5. Matrix Representation of the Scattering Cross Section

The scattering cross section matrix is defined by letting

$$\Sigma_{s,q,q'} = \operatorname{diag}(\sigma_{s,q,q',111}, \dots, \sigma_{s,q,q',KJM}). \tag{A.29}$$

The scattering cross section for all energy groups is then

$$\Sigma_{s} \equiv I_{L} \otimes \begin{pmatrix} \Sigma_{s,11} & \dots & \Sigma_{s,1G} \\ \vdots & \ddots & \vdots \\ \Sigma_{s,G1} & \dots & \Sigma_{s,GG} \end{pmatrix}. \tag{A.30}$$

The full scattering operator \mathbb{S} is then

$$\mathbb{S} = (I_G \otimes I_L \otimes Z) (I_G \otimes L^{0,+}) \Sigma_s (I_G \otimes L^0) (I_G \otimes I_L \otimes S). \tag{A.31}$$

Appendix A.3.6. Matrix Representation of the Fission Cross Section

The fission cross section matrix is defined similarly

$$\Sigma_{f,g,g'} \equiv \operatorname{diag}(\chi_{g'g}\nu\sigma_{f,g',111},\dots,\chi_{g'g}\nu\sigma_{f,g',KJM}),\tag{A.32}$$

where the fission cross section for all energy groups is then

$$\Sigma_{f} \equiv I_{L} \otimes \begin{pmatrix} \Sigma_{f,11} & \dots & \Sigma_{f,1G} \\ \vdots & \ddots & \vdots \\ \Sigma_{f,G1} & \dots & \Sigma_{f,GG} \end{pmatrix}. \tag{A.33}$$

The fission operator \mathbb{F} is then

$$\mathbb{F} = (I_G \otimes I_L \otimes Z) (I_G \otimes L^{0,+}) \Sigma_f (I_G \otimes L^0) (I_G \otimes I_L \otimes S). \tag{A.34}$$

Appendix A.3.7. Matrix Representation of the Inverse Neutron Group Velocity

The inverse velocity cross section matrices for energy group g over all cells is given by

$$V_g^{-1} \equiv \frac{1}{v_g} I_{KJM} \in \mathbb{R}^{KJM \times KJM}, \tag{A.35}$$

where I is identity matrix with size KJM. The inverse velocity matrix for all energy groups is then

$$\mathbb{V}^{-1} = (I_G \otimes I_L \otimes Z) \left(I_L \otimes \operatorname{diag}(V_1^{-1}, \dots, V_G^{-1}) \right) (I_G \otimes I_L \otimes S). \tag{A.36}$$

Appendix B.

Appendix B.1. Notation, basic definitions, and operations with tensors

Let d be a positive integer. A d-dimensional tensor $\mathcal{A} \in \mathbb{R}^{n_1 \times n_2 \times ... \times n_d}$ is a multi-dimensional array with d indices and n_k elements in the k-th direction, k = 1, 2, ..., d being the dimensional index. We say that the number of dimensions d is the *order of the tensor*. As usual, we refer to one-dimensional tensors as *vectors*, and two-dimensional tensors as *matrices*. We denote the tensors using uppercase, calligraphic fonts, e.g., \mathcal{A} ; the matrices with bold, uppercase fonts, e.g., \mathcal{A} ; the vectors with bold, lowercase fonts, e.g., \mathcal{A} . To denote tensor's, matrix's, and vector's components, we use both the subscripted notation, e.g., $\mathcal{A} = (\mathcal{A}_{ijk})$, $\mathbf{a} = (a_i)$, $\mathbf{A} = (A_{ij})$, and the MATLAB© [41] notation, e.g.,

$$A := (A(i_1, i_2, \dots, i_d)), \quad i_k = 1, \dots, n_k, \quad k = 1, \dots, d;$$
 (B.1)

$$\mathbf{A} = (\mathbf{A}(i,j)) \in \mathbb{R}^{m \times n} \text{ and } i = 1, \dots, m, j = 1, \dots, n; \mathbf{a} = (\mathbf{a}(i)) \in \mathbb{R}^n \text{ and } i = 1, \dots, n.$$

We form a tensor subarray by fixing one or more of its indices. For example, the *tensor* fibers (the higher-order analog of matrix rows or columns) are defined by fixing all but one of the tensor indices, while the *tensor slices* are two-dimensional sections, defined by fixing all but two of the tensor indices. For example, still using a MATLAB-like notation, $\mathcal{A}(i_1, i_2, :)$ and $\mathcal{A}(i_1, :, :)$ respectively denote the fiber along the third direction and the slice for any fixed index value i_1 .

Appendix B.1.1. Kronecker product

The Kronecker product \bigotimes of matrix $\mathbf{A} = (a_{ij}) \in \mathbb{R}^{m_A \times n_A}$ and matrix $\mathbf{B} = (b_{ij}) \in \mathbb{R}^{m_B \times n_B}$ is the matrix $\mathbf{A} \otimes \mathbf{B}$ of size $N_{\mathbf{A} \otimes \mathbf{B}} = (m_A m_B) \times (n_A n_B)$ defined as:

$$\mathbf{A} \otimes \mathbf{B} = \begin{bmatrix} a_{11}\mathbf{B} & a_{12}\mathbf{B} & \cdots & a_{1n_A}\mathbf{B} \\ a_{21}\mathbf{B} & a_{22}\mathbf{B} & \cdots & a_{2n_A}\mathbf{B} \\ \vdots & \vdots & \ddots & \vdots \\ a_{m_A}\mathbf{1}\mathbf{B} & a_{m_A}\mathbf{2}\mathbf{B} & \cdots & a_{In_A}\mathbf{B} \end{bmatrix}.$$
 (B.2)

Equivalently, it holds that $(\mathbf{A} \otimes \mathbf{B})_{ij} = a_{i_A j_A} b_{i_B j_B}$, where $i = i_B + (i_A - 1) m_B$, $j = j_B + (j_A - 1) m_B$, with $i_A = 1, \ldots, m_A$, $j_A = 1, \ldots, n_A$, $i_B = 1, \ldots, m_B$, and $j_B = 1, \ldots, n_B$.

Appendix B.1.2. Tensor product

There is a relation between Kronecker product and tensor product: Kronecker product is a particular bilinear map on a pair of vector spaces consisting of matrices of a given dimensions (it requires a choice of basis), while the tensor product is a universal bilinear map on a pair of vector spaces of any sort (i.e., it is more general).

Here we define the tensor product of two vectors $\mathbf{a} = (a_i) \in \mathbb{R}^{n_A}$ and $\mathbf{b} = (b_i) \in \mathbb{R}^{n_B}$, which produces the matrix $(\mathbf{a} \circ \mathbf{b})$ of size $N_{\mathbf{a} \circ \mathbf{b}} = n_A \times n_B$ defined as:

$$(\mathbf{a} \circ \mathbf{b})_{ij} = a_i b_j$$
 $i = 1, 2, \dots, n_A, j = 1, 2, \dots, n_B.$ (B.3)

Note that $\mathbf{a} \circ \mathbf{b} = \mathbf{a} \otimes \mathbf{b}^T$. Similarly, the tensor product of matrix $\mathbf{A} = (a_{ij}) \in \mathbb{R}^{m_A \times n_A}$ and matrix $\mathbf{B} = (b_{kl}) \in \mathbb{R}^{m_B \times n_B}$ produces the four-dimensional tensor of size $N_{\mathbf{A} \circ \mathbf{B}} = m_A \times n_A \times m_B \times n_B$, with elements:

$$(\mathbf{A} \circ \mathbf{B})_{ijkl} = a_{ij}b_{kl}, \tag{B.4}$$

for $i = 1, 2, ..., m_A, j = 1, 2, ..., n_A, k = 1, 2, ..., m_B, l = 1, 2, ..., n_B$.

Appendix B.1.3. Contraction of a tensor with a vector

Consider the tensor $\mathcal{X} \in \mathbb{R}^{n_1 \times n_2 \times \cdots \times n_d}$ and the vector $\mathbf{v} \in \mathbb{R}^{n_k}$ for some $1 \leq k \leq d$. The k-th tensor-vector contraction of \mathcal{X} with \mathbf{v} is the summation over the k-th index of the tensor elements weighted by the vector components:

$$(\mathcal{X} \bar{\times}_{k} \mathbf{v})(i_{1}, i_{2}, \dots, i_{k-1}, i_{k+1}, \dots i_{d}) = \sum_{i_{k}=1}^{n_{k}} \mathcal{X}(i_{1}, i_{2}, \dots, i_{k-1}, i_{k}, i_{k+1}, \dots i_{d}) \mathbf{v}(i_{k}).$$
(B.5)

Tensor $\mathcal{X}_{\mathbf{k}\mathbf{v}}$ is a (d-1)-dimensional array of size $N_{\mathcal{X}_{\mathbf{k}\mathbf{v}}} = n_1 \times n_2 \times \ldots \times n_{k-1} \times n_{k+1} \times \ldots \times n_d$.

Appendix B.1.4. The n-mode product

Consider the tensor $\mathcal{X} \in \mathbb{R}^{n_1 \times n_2 \times \cdots \times n_d}$ and the matrix $\mathbf{U} \in \mathbb{R}^{n_U \times n_n}$. The *n*-mode product between \mathcal{X} and \mathbf{U} is the contraction along the *n*-th direction given by

$$(\mathcal{X} \times_n \mathbf{U})(i_1, \dots, i_{n-1}, \ell, i_{n+1}, \dots, i_d) =$$

$$= \sum_{j=1}^{n_n} \mathcal{X}(i_1, \dots, i_{n-1}, j, i_{n+1}, \dots, i_d) \mathbf{U}(\ell, j) \quad \forall \ell = 1, 2, \dots, n_U.$$

Tensor $\mathcal{X} \times_n \mathbf{U}$ has the same dimension d of \mathcal{X} , but size $N_{\mathcal{X} \times_n \mathbf{U}} = n_1 \times n_2 \times \ldots \times n_{n-1} \times n_U \times n_{n+1} \times n_d$ instead of $N_{\mathcal{X}} = n_1 \times n_2 \times \ldots n_d$, which is the size of \mathcal{X} .

Appendix B.2. Differential Operators in TT format.

Applying, for example, the first-order accurate, forward difference formula to approximate the differentiation of $f(x_1, x_2, x_3, x_4)$ through the values of tensor \mathcal{F} along the direction of the independent variable x_2 yields:

$$\left(\frac{\partial f}{\partial x_2}\right)_{i_1,i_2,i_3,i_4} = \frac{\mathcal{F}(i_1,i_2+1,i_3,i_4) - \mathcal{F}(i_1,i_2,i_3,i_4)}{\Delta x_2} + \mathcal{O}(\Delta x_2),$$

for $i_2 = 1, 2, \ldots, (n_2 - 1)$, and where Δx_2 is the grid step-size along the direction of the independent variable x_2 . When working with grid functions, all the discrete analogs of the differential operators (i.e., gradient, curl, divergence, Laplacian, etc.) must be expressed in TT format. Because of the discrete separation of variables provided by the TT format, the forward difference scheme approximating $\partial f/\partial x_2$ is acting only on the index i_2 of the second TT core $\mathcal{G}_2(:,i_2,:)$ of \mathcal{G}^{TT} and can be computed directly in the TT format as follows:

$$\left(\frac{\partial f}{\partial x_{2}}\right)_{i_{1},i_{2},i_{3},i_{4}}^{TT} = \sum_{\alpha_{1},\alpha_{2},\alpha_{3}=1}^{r_{1},r_{2},r_{3}} \mathcal{G}_{1}(1,i_{1},\alpha_{1}) \frac{\mathcal{G}_{2}(\alpha_{1},i_{2}+1,\alpha_{2}) - \mathcal{G}_{2}(\alpha_{1},i_{2},\alpha_{2})}{\Delta x_{2}} \dots$$

$$\dots \mathcal{G}_{3}(\alpha_{2},i_{3},\alpha_{3}) \mathcal{G}_{4}(\alpha_{3},i_{4},1) + \varepsilon,$$

where the "dots" denote the continuation line and tensor ε depends on the approximation errors from the tensor train factorization and the finite difference formula. Using the n-mode product introduced in Section Appendix B.1.4, we reformulate this differentiation operator, in TT format as:

$$\left(\frac{\partial f}{\partial x_2}\right)^{TT}(i_1, i_2, i_3, i_4) = \mathcal{G}_1(i_1)(\mathcal{G}_2 \times_2 \mathbf{Diff})(i_2)\mathcal{G}_3(i_3)\mathcal{G}_4(i_4) + \varepsilon \quad \forall i_2 = 1, 2, \dots, (n_2 - 1),$$

where matrix **Diff** is given by,

$$\mathbf{Diff} \equiv \frac{1}{\Delta x_2} \begin{pmatrix} -1 & 1 \\ & \ddots & \ddots \\ & & -1 & 1 \end{pmatrix}. \tag{B.6}$$

Using this format, we apply the forward difference operation matrix **Diff** only along the mode index i_2 of the second core $\mathcal{G}_2(:,i_2,:)$ of \mathcal{G}^{TT} , see, e.g., Fig. 5. The computational cost is greatly reduced by differentiating the multidimensional tensor \mathcal{F} to differentiating only the core \mathcal{G}_2 of the TT tensor \mathcal{G}^{TT} . Importantly, this operation does not modify the ranks of \mathcal{G}^{TT} ; hence, no rounding operation is required to control the rank growth.

Appendix B.3. Integration Operators in TT format.

Consider again the function $f(x_1, x_2, x_3, x_4)$ and its full grid tensor representation $\mathcal{F}(i_1, i_2, i_3, i_4)$ on a four-dimensional, regular, Cartesian grid covering the integration domain $\mathcal{D} = \mathcal{D}_1 \times \mathcal{D}_2 \times \mathcal{D}_3 \times \mathcal{D}_4$, where each \mathcal{D}_k , k = 1, 2, 3, 4, is a 1D, bounded subinterval of \mathbb{R} . Assuming that the nodes over the domain \mathcal{D}_2 of x_2 , are chosen from a quadrature rule with corresponding weights $\mathbf{w} = (w_1, w_2, \dots, w_{n_2})$, we numerically integrate along the independent variable x_2 as follows:

$$\left(\int_{\mathcal{D}_2} f(x_1, x_2, x_3, x_4) dx_2\right)_{i_1, i_3, i_4}^{TT} = \sum_{\alpha_1, \alpha_2, \alpha_3 = 1}^{r_1, r_2, r_3} \mathcal{G}_1(1, i_1, \alpha_1) \left(\sum_{i_2 = 1}^{n_2} w_{i_2} \mathcal{G}_2(\alpha_1, i_2, \alpha_2)\right) \dots \\ \dots \mathcal{G}_3(\alpha_2, i_3, \alpha_3) \mathcal{G}_4(\alpha_3, i_4, 1) + \varepsilon,$$

where the "dots" again denote the continuation line and tensor ε includes the approximation errors from the tensor train factorization of \mathcal{F} and the numerical integration. The numerical integration along x_2 returns a three-dimensional array since the index i_2 is absorbed by the quadrature rule summation. The superindex TT on the left indicates that the tensor collecting the resulting integrals still depends on indices i_1, i_3, i_4 and is in the TT format. Using the contraction product introduced in Section Appendix B.1.3, we rewrite the quadrature rule in TT format as

$$\left(\int_{x_2} f(x_1, x_2, x_3, x_4) dx_2\right)_{i_1, i_3, i_4}^{TT} = \mathbf{G}_1(i_1) \left(\mathcal{G}_2 \bar{\times}_2 \mathbf{w}\right) \mathbf{G}_3(i_3) \mathbf{G}_4(i_4).$$

Like numerical differentiation, numerical integration does not modify the TT ranks of \mathcal{G}^{TT} ; hence, no rounding operation is required to control rank growth. Furthermore, the contraction product $\mathcal{G}_2 \bar{\times}_2 \mathbf{w}$ is an $r_1 \times r_2$ matrix that can be merged to either \mathcal{G}_1 or \mathcal{G}_3 to create the three-dimensional TT-format representation of the tensor collecting such integrals.

Appendix B.4. Interpolation Operators in TT format.

Interpolation refers to the process of estimating the values of a function at every point that lies inside its domain of definition using the values of that function evaluated at suitable grid nodes. We let $\mathcal{I}p_{\xi}$ denote an interpolation operator acting only in the ξ -th direction. For example, we consider the average operator $\mathcal{I}p_2\mathcal{F}$ along the second direction so that

$$(\mathcal{I}p_2\mathcal{F})(i_1, i_2, i_3, i_4) := \frac{\mathcal{F}(i_1, i_2 + 1, i_3, i_4) + \mathcal{F}(i_1, i_2, i_3, i_4)}{2}$$
$$\approx f(x_1(i_1), x_2(i_2) + \Delta x_2/2, x_3(i_3), x_4(i_4)).$$

where $(x_1(i_1), x_2(i_2), x_3(i_3), x_4(i_4))$ is the coordinate vector of the grid node labeled by the multiindex (i_1, i_2, i_3, i_4) and Δx_2 is the grid stepsize along the direction of x_2 . In the TT format, we compute the TT-interpolation scheme $((\mathcal{I}p_2\mathcal{G}^{TT}) \approx ((\mathcal{I}p_2\mathcal{F})^{TT})^{TT}$ from the values of tensor \mathcal{G}^{TT} as follows:

$$((\mathcal{I}p_2\mathcal{G}^{TT})(i_1, i_2, i_3, i_4) := \sum_{\alpha_1, \alpha_2, \alpha_3 = 1}^{r_1, r_2, r_3} \mathcal{G}_1(1, i_1, \alpha_1) \frac{\mathcal{G}_2(\alpha_1, i_2 + 1, \alpha_2) + \mathcal{G}_2(\alpha_1, i_2, \alpha_2)}{2} \dots$$

$$\dots \mathcal{G}_3(\alpha_2, i_3, \alpha_3) \mathcal{G}_4(\alpha_3, i_4, 1) + \varepsilon,$$

where the "dots" again denote the continuation line and ε is the error depending on the TT factorization and the interpolation scheme. The *n*-mode product of Section (Appendix B.1.4) makes it possible to reformulate the action of the interpolation operator ($\mathcal{I}p_2$ in the compact TT matrix format as:

$$((\mathcal{I}p_2\mathcal{G}^{TT})(i_1, i_2, i_3, i_4) = \mathbf{G}_1(i_1)(\mathcal{G}_2 \times_2 \mathbf{I_2})(i_2)\mathbf{G}_3(i_3)\mathbf{G}_4(i_4),$$

where

$$\mathbf{I_p} \equiv \frac{1}{2} \begin{pmatrix} 1 & 1 & & \\ & \ddots & \ddots & \\ & & 1 & 1 \end{pmatrix}.$$

Again, the discrete separation of the mode indices provided by the TT-format representation allows us to apply the interpolation matrix $\mathbf{I_2}$ to the mode index i_2 of the second core $\mathcal{G}_2(:,i_2,:)$. As noted in the case of numerical differentiation and integration, tensor $(\mathcal{I}p_2\mathcal{F}^{TT})$ is already in TT format and the interpolation operation does not modify the ranks of \mathcal{G}^{TT} ; hence, no rounding operation is required to reduce the TT ranks.